Development of Response Spectral Ground-Motion Prediction Equation (GMPE) from Empirical Fourier Spectral and Duration Models

AUTHORS			REVIEW			APPROVAL		
NOM	DATE	VISA	NOM	DATE	VISA	NOM	DATE	VISA
Sanjay Sigh BORA Univ. Potsdam			Pierre-Yves BARD					
			David BAUMONT					

DISSEMINATION: *Authors; Steering Committee; Work Package leaders, Scientific Committee, Archiving.*

Development of Response Spectral Ground-Motion Prediction Equation (GMPE) from Empirical Fourier Spectral and Duration Models

Sanjay Singh Bora

Summary

Often, the empirical GMPEs (Ground-Motion Prediction Equations) developed in the context of seismic hazard analysis require adjustments to make them appropriate for the site in question. This document presents a holistic framework for the development of a response spectral GMPE that is easily adjustable to different seismological conditions, and which does not suffer from the practical problems associated with adjustment in the response spectral domain. The approach for developing a response spectral GMPE is unique as it combines the predictions of empirical models for the two model components that characterize the spectral and temporal behavior of the ground-motion. Essentially, the approach consists of an empirical model for the Fourier amplitude spectrum (FAS) and a model for the ground-motion duration. These two components are combined within the random-vibration theory (RVT) framework to obtain predictions of response spectral ordinates. Additionally, FAS corresponding to individual acceleration records are extrapolated beyond the useable frequencies using the stochastic FAS model, obtained by inversion as described in Edwards & Faeh, (2013). To that end, a (oscillator) frequency dependent duration model, consistent with the empirical FAS model, is also derived. A subset of the RESORCE-2012 database is considered for the present analysis. Additionally, results on the application of the present approach for performing the host-to-target adjustments in-terms of site conditions at two given test sites are also presented. Besides its flexibility for application in a range of seismic hazard studies, a significant reduction in aleatory variability ($\sigma<0.5$ in natural log units) at shorter periods brands the presented approach as a potentially viable alternative to classical GMPEs based on regression of response spectral ordinates.

Contents

1. RESORCE-2012 database

For the present analysis, the data has been taken from the RESORCE-2012 strong-motion database compiled in the framework of the SIGMA project. This entire database comprises the 5115 processed recordings from 1685 events recorded at strong motion stations around Europe, the Mediterranean region, the Middle East and some parts of central Asia as well. However, a subset of the entire database was considered for presented analysis. It is a usual practice in studies involved with the GMPE development to select a dataset based on a criteria adopted by the equation developer.

1.1 Data selection

The general approach for selecting the dataset which was considered useful for the presented analysis was to include all the earthquakes and records except,

- events for which the moment magnitude was not reported,
- events for which $M_W<4$.
- Any event which is not representative of shallow crustal event i.e. hypocentral distance > 30 km,
- any event with no information of the style of faulting,
- any record not having either of the two horizontal components,
- any record for which the Joyner-Boore distance is not reported,
- any record for which the shear-wave velocity V_{S30} was not reported,
- any record at a distance (Joyner-Boore) greater than 200km,
- two records having consecutive spikes in their accelerograms were also removed from the dataset.

Often filters are used to reduce the effect of spurious noise present in a record at both the lower and higher ends of its spectrum (Boore & Bommer, 2005). The high-pass frequency of a filter indicates that frequency above which all the frequencies are allowed to pass by filtering action; and similarly the low-pass frequency indicates the frequency below which all the frequencies are allowed to pass. Sometimes it has been observed that there is an over filtering at the lower frequency end of the spectrum which affects the records, particularly those originating from large magnitude earthquakes. Therefore, in addition to the above criteria, those records in the present study were also not considered for which the high-pass frequency of the filter was found to be larger than Brune's source-corner frequency for an average stress drop of 10 MPa. Consequently the application of these criteria resulted in a dataset of 1232 records recorded at source-to-

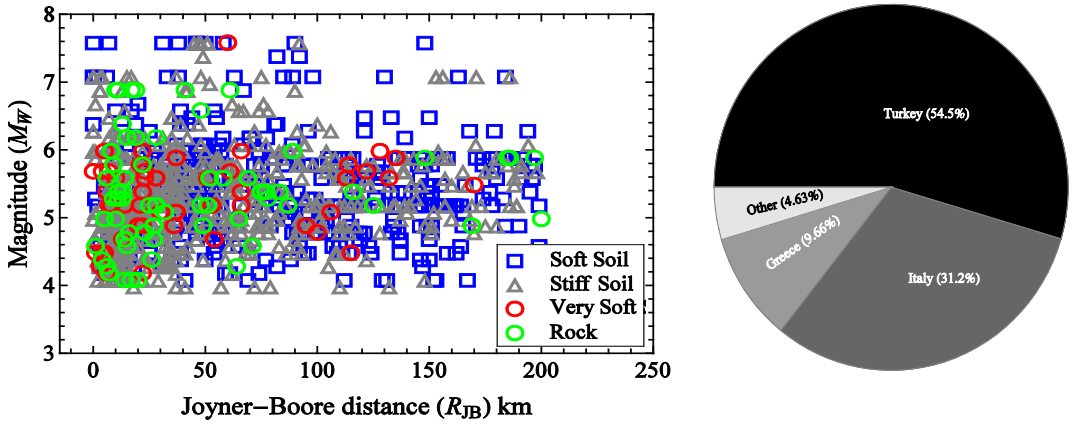

Figure 1 *Left*,Magnitude and distance distribution of the dataset used in the presented study corresponding to different site conditons beneath the recording station. *Right*, the Pie chart indicates relative contributions of the records from different countries.

distance of $R_{JB} \leq 200$ km from 369 earthquakes with a moment magnitude in the range $4.0 \leq M_W \leq 7.6$. The magnitude-distance distribution of the selected dataset pertaining to different site conditions is depicted in Figure 1. The site conditions were classified according to the average shear-wave velocity in the uppermost 30 m beneath the recording site (V_{s30}). Solely for the purpose of this figure, the sites observed to have V_{s30} values above 750 m/sec were classified as

rock, those with values between 360 and 750 m/sec as stiff soil, those with the values between 180 and 360 m/sec as soft soil and the sites with V_{s30} values below 180 m/sec were classified as the very soft soil class. The pie chart in Figure 1 indicates the relative contribution of the records from different countries in the selected dataset.

2. Essence of the approach

The basis of developing a response spectral GMPE presented in this study lies within the random vibration theory (RVT) framework (Cartwright and Longuet-Higgins, 1956) which was successfully used by (Boore, 2003) for the prediction of response spectral ordinates for an input ground motion of finite duration. Typically the calculation of response spectral ordinates through RVT involves the use of the FAS and an independent estimate of ground- motion duration. Therefore, the presented approach of developing a response spectral GMPE consists of deriving two empirical models for FAS and duration of ground-motion which are combined within the RVT framework to obtain the response spectral ordinates (Bora et al., 2014). Additionally, in order to extend the useable frequency range of the empirical FAS model a stochastic model based extrapolation of individual FAS is proposed, that essentially predicts the Fourier amplitudes beyond the frequencies supported in the observed data. It is common when processing accelerograms to assign certain limiting values of frequency that define the usable frequency range. These limiting frequencies are generally dictated by either the available sampling rate or by the ambient noise present at low and/or high frequencies. Outside of this range the observed spectrum is not deemed representative of the actual ground-motion and only the ordinates corresponding to the usable amplitudes are used for deriving the empirical FAS model. Therefore, the number of data-points available for regression analysis tends to vary with frequency and the sampling of the predictor variables (of magnitude and distance, etc.) will also

vary with frequency as a result. The extrapolation scheme being presented here essentially predicts the Fourier spectral amplitudes beyond the frequencies which are supported in the observed data corresponding to individual accelerograms. This scheme requires the determination of stochastic model parameters those are most appropriate for individual spectra. The extrapolated Fourier spectral ordinates are used to derive an empirical FAS model at a wide range of frequencies i.e. well beyond the frequencies ordinates available in the observed spectra.

Moreover an oscillator-frequency dependent duration model is also derived. For the purpose, the duration (D_{gm}) of ground-motion is determined at each oscillator-frequency corresponding to a single-degree-of-freedom system (SDOF) with 5% critical damping. As mentioned in Bora et al. (2014), in order to determine the D_{gm}, it is treated as the variable to minimize the misfit between the observed response spectral ordinate and RVT based response spectral ordinate at each oscillator frequency. Although, the detailed analysis and equations involved in the determination of D_{gm} and for the forward computation of response spectra will be discussed in the following sections, a flow-chart depicting the entire scheme of the presented approach is shown in Figure 2.

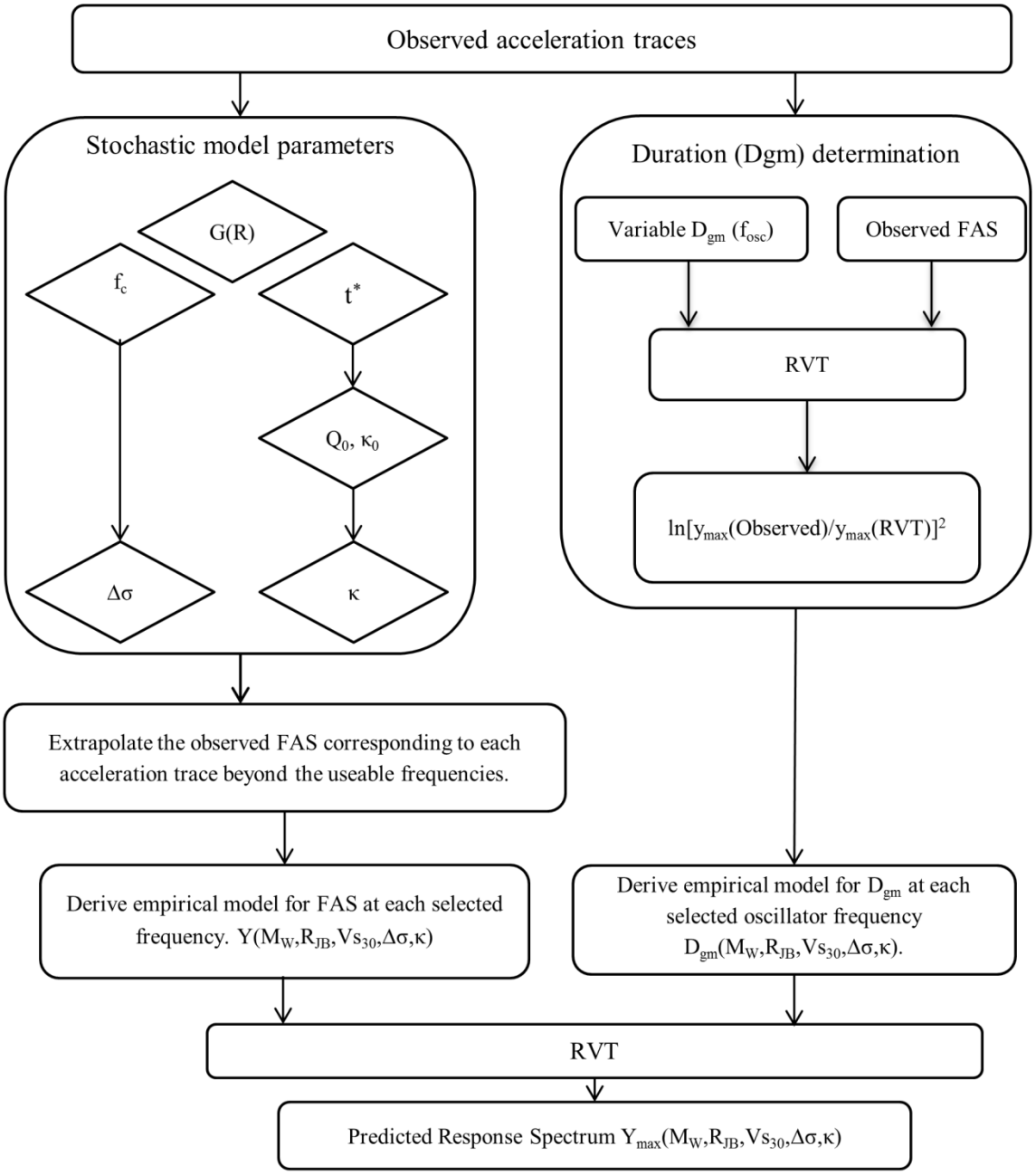

Figure 2 A schematic flow-chart of the presnet method for developing a response spectral GMPE.

3. Determination of stochastic model parameters

The stochastic ground-motion simulation technique has been used in many parts of the world in order to model high-frequency ground-motions of engineering interest (e.g. Atkinson & Boore, 2006; Edwards & Faeh, 2013; Rietbrock et al., 2013) . This simulation technique employs a

simple yet powerful analytical relationship to model the far-field acceleration spectrum of the ground-motion using the Brune's source model (Brune,1970; 1971). Subsequently, this source model is modified to accommodate the propagation and site effects on the ground-motions obtained at a site as given in the following equation,

$$Y(f) = CM_0G(R)\left[\frac{(2\pi f)^2}{1+\left(\frac{f}{f_c}\right)^2}\right]A(f)\exp(-\pi f t^*) \qquad (1),$$

where M_0 is the seismic moment in units of N-m and f_c is the corner frequency in Hertz, which is given by $f_c = 0.4906\beta(\Delta\sigma/M_0)^{1/3}$ (Eshelby, 1957), where $\Delta\sigma$ is the stress parameter in MPa and β (=3.5 km/s) is the shear-wave velocity near the source. The constant C is generally taken as $C=\Theta_{\lambda\varphi}F\xi/(4\pi\rho\beta^3)$ (Brune, 1970), where $\Theta_{\lambda\varphi}$(=0.55) is the average radiation pattern for S-waves (Boore & Boatwright, 1984), F(=2.0) is the free surface amplification, ξ(=1/√2) is a factor to account for the average ratio of vertical-horizontal ground-motion amplitudes and ρ(=2800 kg/m^3) is the density (Boore, 1983; 2003) .

In equation (1) G(R) is the geometrical spreading function, which represents the frequency-independent decay of Fourier amplitudes as a function of distance. In theory it should equal 1/R for an isotropic homogenous whole space, but usually it has been found to be a complex function of distance (Atkinson & Mereu, 1992; Campillo et al., 1984). At short distances, the geometric spreading is controlled by the decay of direct body-wave amplitudes in a layered crust model, while at greater distances there can be contributions from a combined effect of reflections and refractions from the Moho and a transition to surface-wave spreading.

Therefore, geometrical spreading represents an attenuation regime in a particular geologic and tectonic setting and is often determined from a dataset with a good sampling in terms of distance.

The attenuation operator (t^*) is a combination of the anelastic attenuation represented by the quality factor (Q_0) and the parameter kappa (κ) as given in the following equation,

$$t^* = \frac{R}{Q_0 \beta} + \kappa \qquad (2)$$

where β the average shear velocity (3.5 km/s) and R the hypocentral distance. The term 'kappa' in equation (2) originally introduced by (Anderson & Hough, 1984) that parameterizes the high-frequency fall-off observed in the real accelerograms. In equation (1), A(f) is a function that reflects the effect of the impedance-contrast during the wave propagation.

As mentioned in the previous section, in order to extrapolate the spectrum corresponding to individual accelerogram components, the stochastic model parameters those are most appropriate for each acceleration trace needed to be determined. However, some of the parameters like geometrical spreading and the quality factor (Q_0) are derived as an average over the entire dataset. Therefore, the general scheme for inverting the acceleration spectra for determining the stochastic model parameters involves: 1) determination of seismic moments and consequently geometrical spreading factor from the entire dataset (e.g., Atkinson and Mereau, 1992), 2) determination of the source corner-frequency (f_c) and the attenuation operator (t^*) for each individual accelerogram component (e.g. Scherbaum, 1990; Thatcher & Hanks, 1973), 3) determination of a dataset average quality factor (Q_0) and a record κ (kappa) from inverted t^* values; and finally, 4) determination of the site amplification effects at each station from the residuals obtained at the second stage. A least-square fit is performed using the natural logarithm of equation (1). In order to solve the nonlinear equation used in the inversion Newton's method was used (implemented in Mathematica). Moreover, only the accelerograms recorded at hypocentral distance $\geq$15 km were considered to enable the far-field approximation to be valid.

This resulted in a reduced dataset with 1115 accelerograms recorded at 339 stations from 347 earthquakes.

3.1 Apparent geometrical spreading

In an attempt to decouple the effects of geometric spreading and anelastic attenuation, first the geometric spreading function was determined separately and prior to the main inversion scheme. Once the model for the geometric spreading is established the other stochastic model parameters are determined in subsequent steps. The low frequency spectral amplitudes were used to determine the rate of apparent spectral decay with distance (r_{hyp}) using a similar scheme as that adopted by Atkinson (2004). Since even at low frequencies large magnitude events have a significant source effect (i.e., low corner-frequency) the Fourier spectral amplitudes at frequencies $0.2 \leq f \leq f_c$ for each record were corrected for an initial estimate of the common source effect. This common source effect was estimated for only those events which are recorded at least at three stations in the distance range $r_{hyp} \leq 70$ km. Here, the common-source effect is determined as an average of source-spectra over the recordings in this distance range. In order to determine the event-specific corner-frequency (f_c) the observed Fourier amplitude spectra in that distance range were inverted using the catalogue moment magnitude and a theoretical decay rate of 1/R. The inversion was performed over the entire band of the spectra which gives an event-specific source-corner frequency (f_c). After determining an inverted source-spectrum for each event at frequencies over the range $0.2 \leq f \leq f_c$, individual spectrum corresponding to that event is corrected for this common-source effect by dividing the observed spectra by the event-specific source spectrum. However, only those events for which the source-corner frequency $0.3 \leq f_c \leq 3$ Hz have been used assuming that $f_c < 0.3$ may not represent the actual source-effect because of the noise present at low frequencies; and $f_c > 3$Hz can be influenced by the anelastic (Q_0) and high-frequency attenuation (κ). The mean of the source-corrected spectral amplitudes over the selected

frequency range are plotted against r_{hyp} in Figure 3. Care was taken to identify apparent breaks in scaling that actually can be attributed to the site effects. In order to obtain the best fit slope in different distance ranges, different combinations of distance ranges including the bilinear form and corresponding slopes were investigated. Finally the distance ranges and corresponding slopes were selected so as to minimize the error in terms of prediction. Therefore, a trilinear form with the slopes 1.27 for $R_{hyp} \leq 50$ km, 0.33 for $50<R_{hyp}\leq 110$ km and 1.29 beyond 110 km was determined from the present dataset.

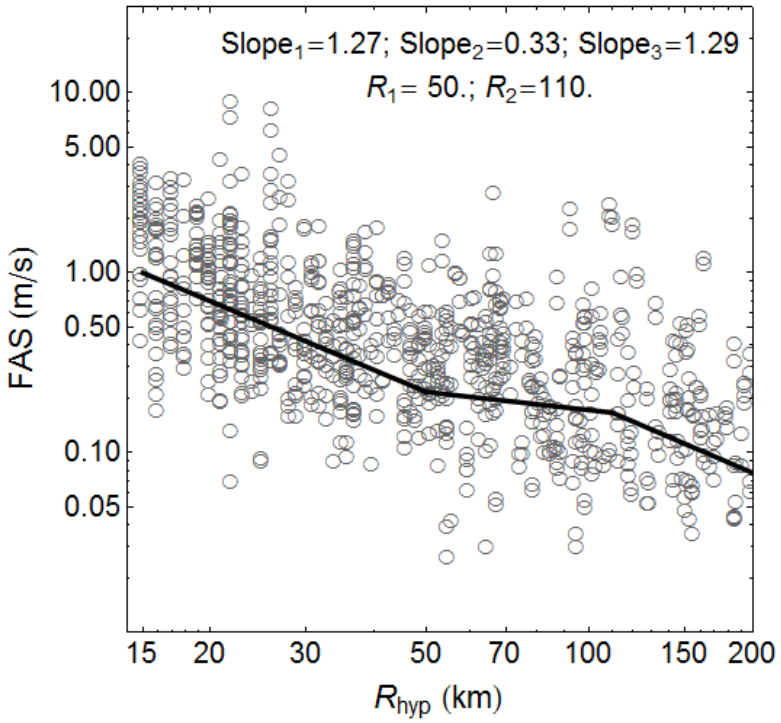

Figure 3 Plot of the (mean) source corrected spectral amplitudes with hypocentral distance.

3.2 Inversion for f_c and t^*

After constraining the model for the geometric spreading, the observed FAS were inverted to determine the attenuation and source parameters. The shape and amplitude of the Fourier spectrum from an observed earthquake at a given distance can be explained in terms of f_c,

seismic moment (M_0) and the combined path-site dependent attenuation operator (t^*). The f_c and t^* are determined for each acceleration record using the entire useable spectrum simultaneously which was termed as the 'broad-band' inversion by Edwards & Faeh (2013). However, at this stage, a record-specific f_c was determined as opposed to the event-specific value determined by Edwards and Faeh (2013). As mentioned earlier the reason for determining the record-specific f_c and t^* is to make the extrapolation consistent with the observed spectrum, rather than focusing on a robust parameter determination.

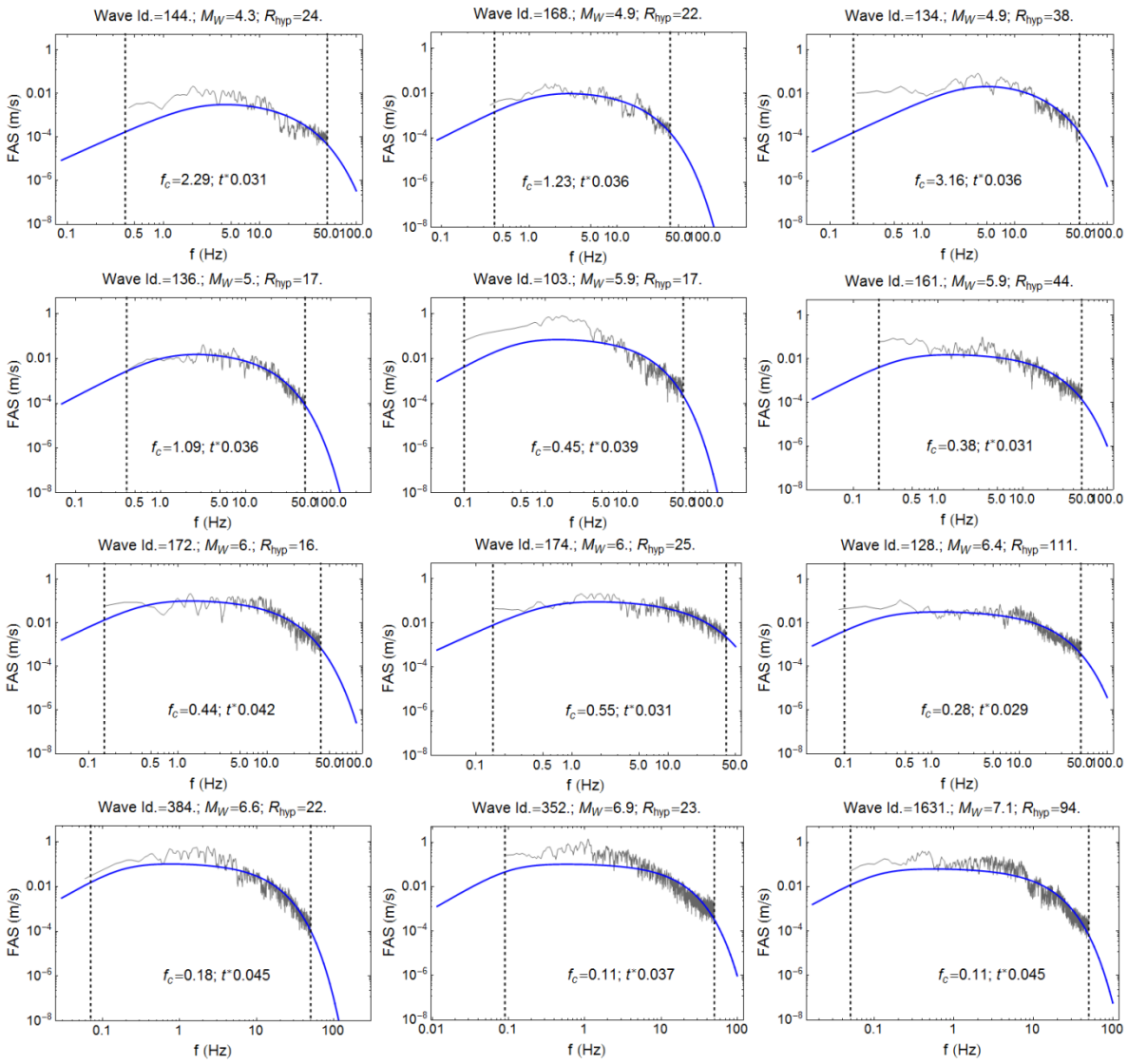

Figure 4 Plot depicting the fit between the rock (Vs_{30}=620 m/s) normalized FAS (thin gray) and modeled FAS (thick blue), vertical dashed lines indicate the lower and upper limits of the useable frequency.

Moreover, physically f_c is expected to vary from record-to-record depending upon the directional and directivity effects (Madariaga, 1976). Therefore, after fixing the geometrical spreading factor the f_c and t^* were allowed to vary for an individual spectrum while using the catalogue based moment magnitude (M_W) and previously determined geometrical spreading model to determine the low frequency spectral level. Source f_c was limited such that it could vary within the $\Delta\sigma$ range 0.1-100 MPa. Similarly, the t^* values were also allowed to vary in a range corresponding to

Q_0= 200-2000 and κ=0.001-0.08s. In addition, observed spectra are adjusted such that they correspond to the same reference shear-wave velocity of 620 m/s (e.g. Boore & Joyner, 1997; Poggi et al., 2011). It was assumed that the generic rock velocity profile of California (Boore and Joyner, 1997) anchored at Vs_{30}= 620 m/s is suitable for the dataset used here. The reference crustal amplification was computed using the quarter wavelength approximation (Boore & Joyner, 1997). Figure 4 depicts the plots of observed FAS normalized to the reference rock (Vs_{30}=620 m/s) and the fitted FAS corresponding to some selected records to demonstrate the representative performance of the fitted model.

3.3 Attenuation (Q_0 and κ)

The combined attenuation operator t^* values obtained from the previous stage were used to decouple the path dependent anelastic attenuation (Q_0) and the high frequency attenuation (κ) commonly attributed to the propagation effects in the uppermost layer of soil and rock beneath the recording site. A straightforward way for determining contributions from Q_0 and κ from the dataset is to perform a linear regression of the inverted t^* values against distance and then relate the obtained coefficients to Q_0 and κ using the relationship given in equation (2). The slope of the fitted line was determined as 0.00026±0.00002 which gives Q_0=1100 with the limits 1016 and 1200. The intercept representing the average site term κ was found to be κ_0=0.0418±0.00189 (s). In order to obtain the record specific values of κ parameter the t^* values were corrected for the distance and the anelastic attenuation Q_0=1100. Hereafter, κ will be referred to the record-specific parameter values, while κ_0 will be referred to the database average obtained as the intercept of the straight line.

3.4 Site amplification

The site amplification curves corresponding to each station were determined using the residuals obtained during the first stage inversion (Edwards et al., 2008; Drouet et al., 2010; Edwards & Faeh, 2013) . The amplification at each frequency was computed as the geometric mean of all the factorial residuals i.e. observed Y(f)/modeled Y(f) at that frequency over all spectra recorded at a given site. This approach has been shown to provide amplification consistent with expected 1D behavior at rock sites, and more complex 2 or 3D behavior at soil (Edwards et al., 2013). The catalogue based moment magnitude was used at the first stage of inversion for determining the low frequency spectral level. In order to use as much data as possible for developing the GMPE, the site amplification curves were computed for all the stations. The selected dataset includes a total of 339 stations; however there are only 143 stations that have ≥3 records.

The generic rock site (Vs_{30}=620 m/s) for which the Fourier spectra have been corrected can be assumed as the reference for the site amplification curves presented in this study, i.e., all amplifications are relative to a site with 620m/s. Figure 5 depicts the site amplification curves for a selection of stations. The site amplification curves presented here are expected to represent multiple effects together, e.g., the actual amplification due to the upper soil layers beneath the station, the residual path effects which could not be modeled and certain other un-modeled phenomena and noise.

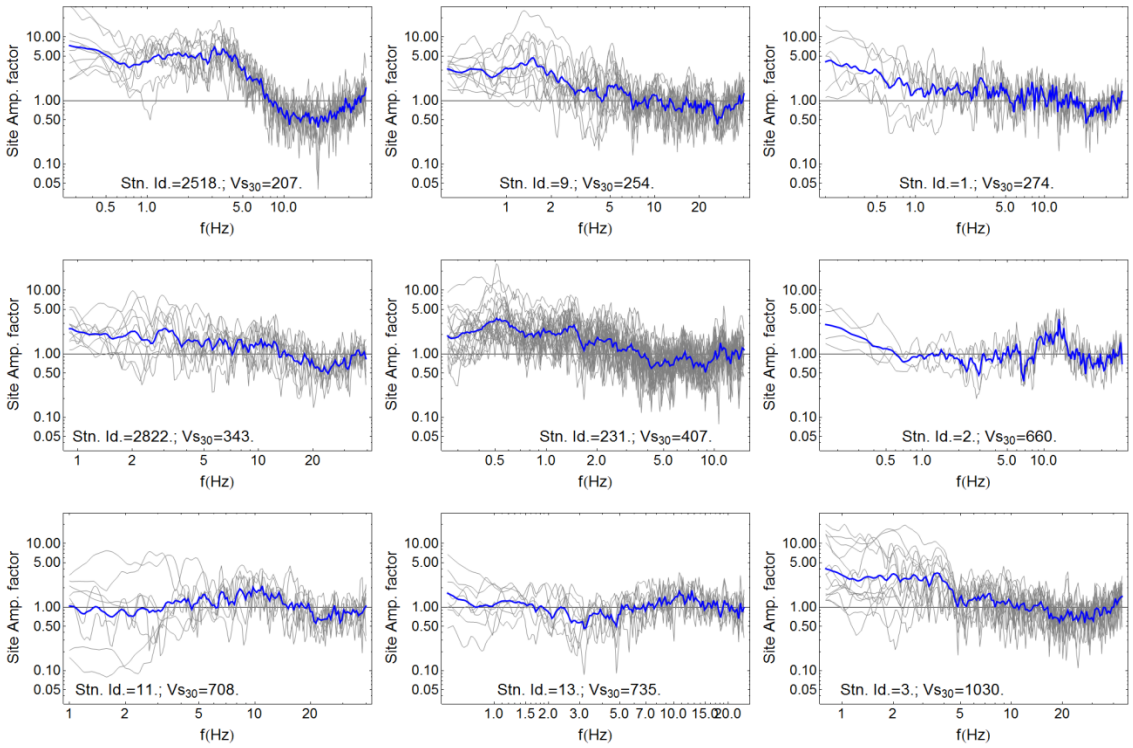

Figure 5 Site amplification curves (thick blue) obtained as the residual analysis for selected stations. Thin gray lines indicate the residuals corresponding to the each record.

3.5 Source parameters f_c and $\Delta\sigma$

Inverted f_c values are plotted against the catalogue moment magnitude in Figure 6. The regression line determined from this dataset gives the following relationship,

$$\mathrm{Log}_{10}(f_c) = 2.66(\pm 0.06) - 0.51(\pm 0.01) \times M_W \qquad (3),$$

which is found to be effectively equivalent to a constant stress-parameter model. The relationship between f_c and M_W for a constant $\Delta\sigma$ model comes out to be,

$$\mathrm{Log}_{10}(f_c) = 2.60(\pm 0.008) - 0.5 \times M_W \qquad (4),$$

which gives a median $\Delta\sigma$ value of 14.5 MPa. The stress parameter corresponding to the inverted f_c (Hz) value can be obtained using the relationship,

$$\Delta\sigma = M_0 \left(\frac{f_c}{0.4906\beta}\right)^3 \quad (5)$$

(Brune, 1970, 1971; Eshelby, 1957) where β is the near-source velocity (assumed to be 3.5 km/s) and as mentioned earlier seismic moment M_0 (N-m) is determined from the moment magnitude in the database using the relationship from (Hanks & Kanamori, 1979).

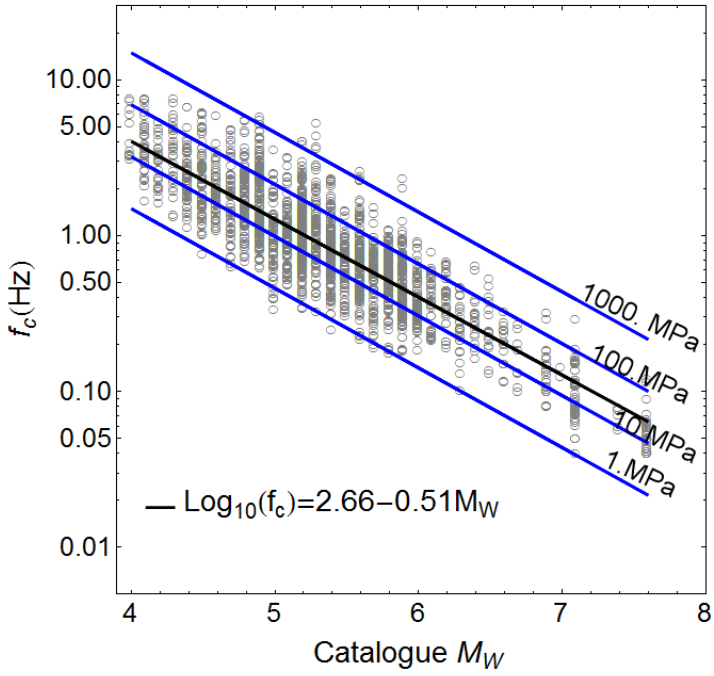

Figure 6 Plot of the inverted source corner frequency (f_c) against magnitude. The thick black line corresponds to the best fit line. Thick blue, lines indicate the lines of constant Δσ.

The stress parameter values Δσ obtained in this study are found to be slightly on the higher side in comparison to the values obtained by Edwards and Faeh (2013). The moment magnitude, M_W, given in the metadata of RESORCE database was used to determine the spectral amplitudes at low frequencies of the spectrum. Therefore, the variability involved in the magnitude estimation may propagate in to the fitted f_c values and hence consequently to the stress parameter.

4. **Extrapolation of the observed FAS**

After determining the stochastic model parameters, the FAS corresponding to each record was extrapolated beyond the filter cut-offs towards low and high frequency ends of the spectrum. For the purpose, the record-specific f_c and t^* values along with the derived geometric spreading function were used. The site-effects in terms of station-specific site amplification curves were used for making the forward prediction. In order to extrapolate the spectrum beyond the upper useable frequency, the spectrum is up-sampled with a common Nyquist frequency of 400 Hz and padded with zeroes beyond the upper usable frequency (Boore & Goulet, 2014).

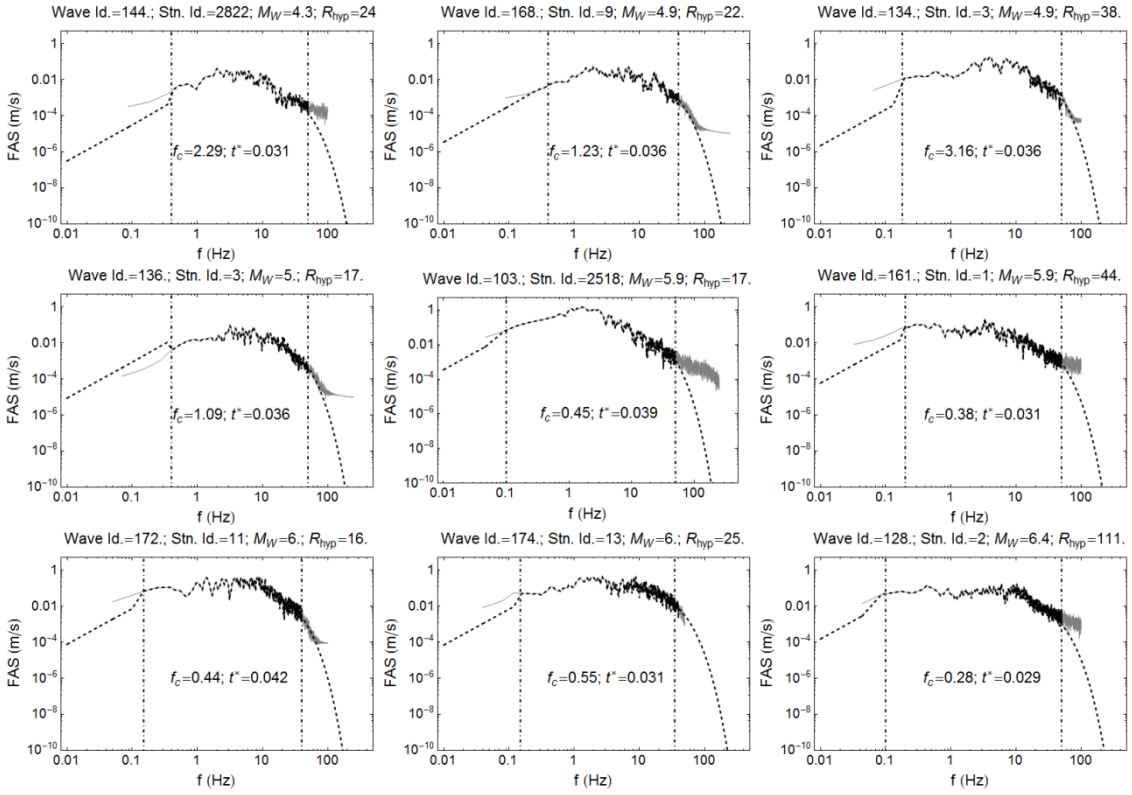

Figure 7 Plots depicting extrapolation of the observed FAS. Thin gray curves indicate the observed FAS and dashed black curves correspond to extrapolated FAS. Vertical dotted-dashed lines depict the lower-and upper limits of the useable frequency respectively. The effect (discontinuity) of station-wise site amplification (shown in Figure 4) on extrapolation can be easily seen at the limits of the useable frequency range.

Subsequently, the padded zeroes were replaced by stochastic model predicted amplitudes in this frequency range. Similarly, for extrapolating towards low frequencies a new minimum frequency (f_2) to be 0.01 Hz was selected and n zeroes were padded between the f_2 and actual minimum frequency where n is given by:

$$n = \frac{1}{dt_{smp} * f_2} - n_0 \quad (6)$$

In equations (6) dt_{samp} is original sampling rate and n_0 is number of data points in the observed record. Subsequently those low frequency padded zeroes were replaced by the stochastic model generated amplitudes. Essentially, for a record, the spectral amplitudes between the useable frequencies were selected as they were given in the observed record; subsequently the model generated amplitudes were used to predict spectral amplitudes beyond the useable frequency on the either sides of the spectrum. Consequently, a FAS corresponding to each record ranging from 0.01 to 400 Hz was obtained. This enables one to use all the frequencies in this range for deriving an empirical model for the FAS. For a subset of records which are depicted in Figure 4, the extrapolated FAS beyond the usable frequency limits along with the observed FAS are depicted in Figure 7.

5. Regression model for the FAS

For deriving the empirical model for the FAS a similar functional form as used in Bora et al. (2014) was chosen. However, a set of three empirical regression equations for FAS of the ground-motion are derived herein. The three regression equations differ in terms of the predictor variables included as follows,

$$\ln Y(f) = c_0 + c_1 M_W + c_2 M_W^2 + (c_3 + c_4 M_W)\ln\left(\sqrt{R_{JB}^2 + c_5^2}\right) - c_6\sqrt{R_{JB}^2 + c_5^2} + c_7 \ln(Vs_{30}), \quad (7)$$

$$\ln Y(f) = c_0 + c_1 M_W + c_2 M_W^2 + (c_3 + c_4 M_W)\ln\left(\sqrt{R_{JB}^2 + c_5^2}\right) - c_6\sqrt{R_{JB}^2 + c_5^2} + c_7 \ln(Vs_{30}) - c_8\kappa, \quad (8)$$

and

$$\ln Y(f) = c_0 + c_1 M_W + c_2 M_W^2 + c_3 \ln(\Delta\sigma) + (c_4 + c_5 M_W)\ln\left(\sqrt{R_{JB}^2 + c_6^2}\right) - c_7\sqrt{R_{JB}^2 + c_6^2} + c_8 \ln(Vs_{30}) - c_9\kappa. \quad (9)$$

In above equations (7-9), Y is the geometric mean of the Fourier spectral amplitude from both the horizontal components at frequency f. The M_W is the moment magnitude; R_{JB} is the closest distance from the recording site to the surface projection of the rupture plane and Vs_{30} is the time-averaged shear-wave velocity in the upper 30 meters of the soil column beneath the recording site. For performing the regression, using the equations (8) and (9), the record-specific values of the predictor variables $\Delta\sigma$ and κ are used. As mentioned earlier, the record-specific f_c values are used to obtain the record specific $\Delta\sigma$ values. Similarly the record-specific κ values are obtained by correcting corresponding t^* for the distance and whole-space attenuation Q_0 using equation (2). The regression coefficients involved in equations (7-9) are determined using the random effects algorithm of Abrahamson & Youngs (1992). This algorithm separates the residuals misfit into between-event and within-event components that are assumed to be normally distributed with zero mean and standard deviation τ and ϕ respectively. The total standard deviation (σ) associated with the median logarithmic Fourier spectral amplitude at each frequency f is computed as follows,

$$\sigma = \sqrt{\tau^2 + \phi^2} \quad (10)$$

The regression was performed on the smoothed Fourier spectral amplitudes at selected frequency ordinates between 0.01-400 Hz. The spacing of 0.04 in natural-log units resulted in 116 frequency ordinates from 0.01-398.11 Hz. For selecting the smoothed Fourier amplitude at a chosen frequency a Gaussian kernel was used which is applied to ordinates at a total of five frequency values (i.e., two either side of the chosen frequency ordinate). The regression was performed at each of the 116 frequencies; values of the coefficients involved in equation (7), (8) and (9) are listed in Table 1, Table 2 and Table 3 respectively. The Tables can be found in the appendix attached to this document. It is worth mentioning here that no smoothing was applied over the coefficients for predicting the FAS. The tables containing the coefficients are given in the attached appendix.

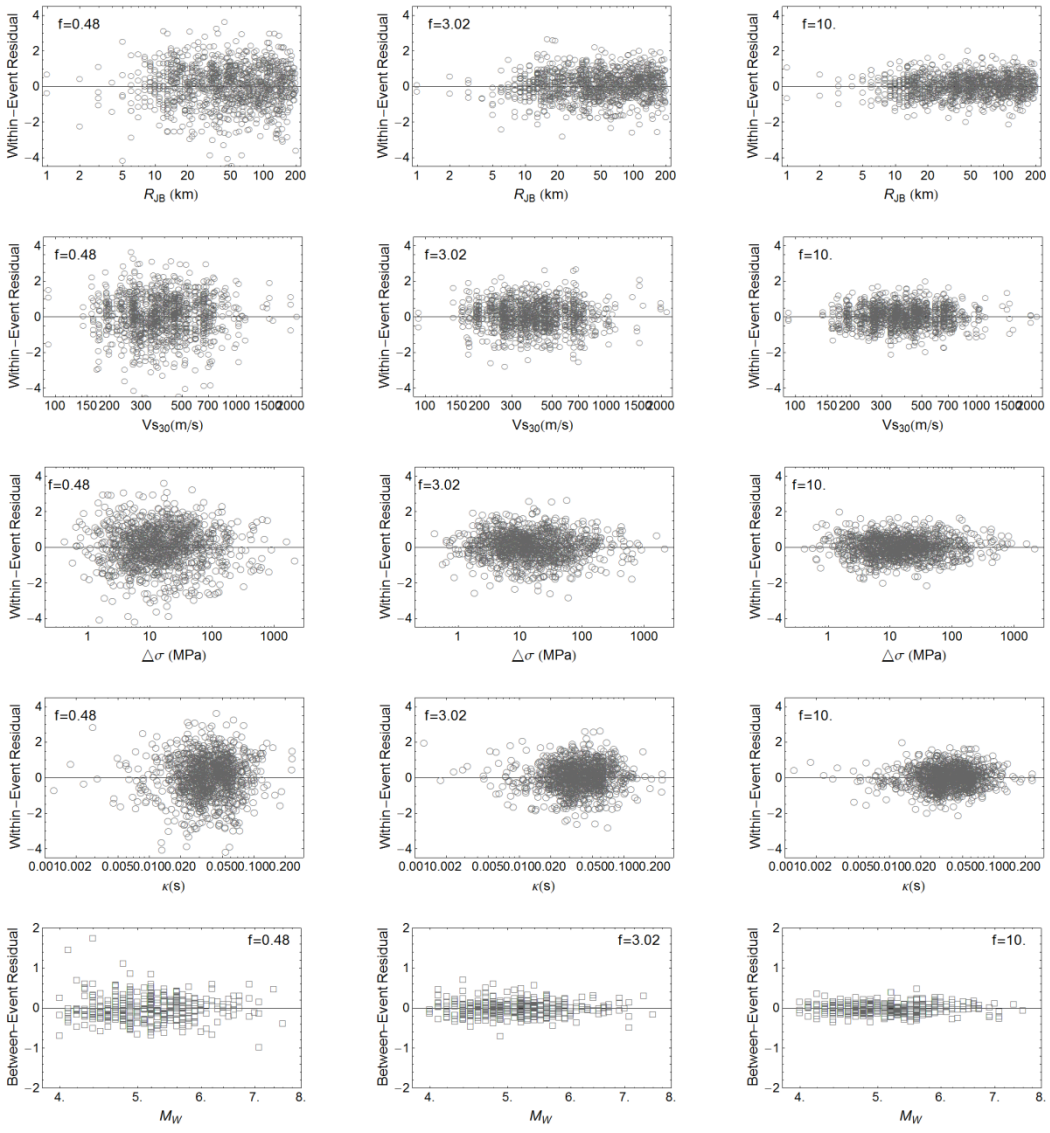

Figure 8 Plot of between- and within-event residuals against M_W, R_{JB}, Vs_{30}, Δσ and κ at f=0.48, 3.02 and 10 Hz.

For checking the robustness of the presented regression models, the regression residuals are plotted against the predictor variables magnitude, distance, Vs_{30}, Δσ and κ involved in equation (9) at f=0.48, 3.02 and 10 Hz and are shown here in Figure 8. The equation (9) is selected to depict the variation of residuals against the predictor variables because it involves the predictor variables of equation (7) and (8). As can be observed from Figure 8, the dispersion of the residuals is observed to decrease towards higher frequencies (at 3 and 10 Hz). The greater

dispersion of the within-event residuals at low frequencies can be attributed mainly to the site amplification effects which could not be modeled through the simple proxy (Vs_{30}) used to account for the site effects in equation (9).

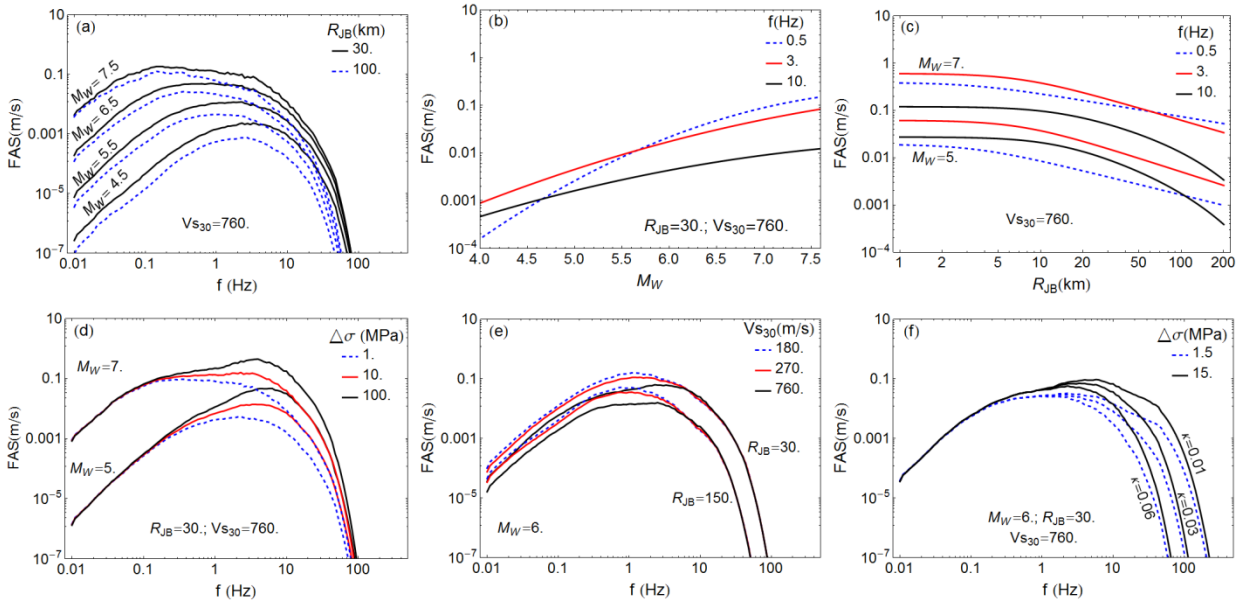

Figure 9 Scaling of model predicted FAS with magnitude is depicted in panel a; panel b depicts the scaling of spectral amplitudes with magnitude, scaling with distance is depicted panel c. Panel d depicts scaling of FAS with Δσ; scaling with Vs_{30} is depicted in panel e, panel f depicts the scaling of FAS with κ.

The scaling of median Fourier amplitude spectra with all the predictor variables involved in equation (9) is depicted in Figure 9. Figure 9a depicts magnitude scaling of the entire spectrum at a distance R_{JB}=30 and 100 km respectively. A magnitude-corner-frequency relationship can be readily observed. Figure 9b depicts the scaling of Fourier spectral ordinates at f=0.5, 3 and 10 Hz. Similarly, Figure 9c represents the scaling of Fourier spectral ordinates at these same frequencies corresponding to magnitude M_W=5 and 7. Panel d of Figure 9 depicts the scaling of the Fourier spectrum with Δσ corresponding to magnitudes M_W=5 and 7.

The influence of the Δσ beyond the corner frequency is visible. Fourier spectral ordinates beyond a certain frequency (5 Hz in this figure), for the similar attenuation conditions, are solely

determined by the $\Delta\sigma$ irrespective of earthquake magnitude. A similar plot is depicted in panel f of the same figure representing scaling of the Fourier spectrum with κ for two different values of $\Delta\sigma$. Often, the $\Delta\sigma$ is observed to control the high frequency amplitudes. However, κ is also expected to reduce the high frequency amplitudes depending upon its magnitude. The scaling of the Fourier spectrum with Vs_{30} is depicted in Figure 9e at two different source-to-site distances R_{JB}=30 and 150 km. The stiffness of the profile is observed to have a larger impact on the low frequency spectral amplitudes than at the high frequency amplitudes. It's worth emphasizing here that, these predictions depicted in Figure 9 are shown for median values of the predicted FAS. However it is believed that RVT method utilizes a mean FAS, hence for obtaining the forward response spectra using the RVT a mean FAS will be used. Although, the Fourier spectral amplitudes can not be considered as independent, this conversion from median to mean FAS will be performed based upon the assumption that the Fourier spectral amplitudes are log-normally distributed at each frequency ordinate.

6. Oscillator-frequency dependent duration (D_{gm}) model

The stochastic simulation method of Boore assumes that the radiated energy from an earthquake source can be characterized by a process exhibiting spectral stationarity with energy released over a duration equal to the rise time (the inverse of the corner frequency, f_c). Moreover, the computation of response spectral ordinates using the RVT method also requires an estimate of ground-motion duration (Boore & Thompson, 2014; Boore, 1983; Hanks & McGuire, 1981; Vanmarcke & Lai, 1980). There are multiple definitions of duration in the literature and the choice of a particular type is driven by its suitability for a particular application (Bommer & Martínez-Pereira, 1999).

Bora et al. (2014) proposed another measure of duration, D_{gm} that is different from most others in that it is not determined directly from the recorded acceleration trace. However, it is tied very closely to the RVT framework. The computation of response spectral ordinates using the RVT method depends upon the FAS (model) and duration of ground-motion (Boore, 2003; Boore & Thompson, 2012; Bora et al., 2014). The duration in this study is defined as having the value that is required in order for a response spectral ordinate computed using RVT, given the FAS of the record, to be equal to that of the observed record. The approach for estimating this duration can be summarized in two steps: 1) compute the FAS from given acceleration trace; 2) use this FAS as the input to RVT and solve for the duration (the only remaining unknown) in such a way that the mismatch between the RVT computed response spectrum and the observed response spectrum is minimized. This process involves minimization of the mismatch between the two response spectral amplitudes (RVT based and observed) at different oscillator frequencies corresponding to a single-degree-of-freedom system (SDOF) with 5% critical damping. This method of duration estimation from an acceleration trace is unique in that it was derived with the purpose of being used within the RVT framework and consistent with the observed response spectra. The choice of an oscillator-frequency dependent duration over a constant duration is to enable the most reliable estimates of the response spectral ordinates. Additionally, an oscillator-frequency dependent duration model will allow making consistent adjustments in duration estimates corresponding to different values of seismological parameters such as $\Delta\sigma$ and κ at a selected oscillator-frequency.

6.1 Determination of duration from acceleration records

As mentioned earlier the computation of response spectral ordinates through RVT method uses the FAS and duration of ground-motion. According to Boore (2003) the response spectral ordinate, y_{max} at any an oscillator frequency f_{osc} is related to the root-mean-square motion, y_{rms}

through a peak-factor, function of the spectral moments and the duration of the input ground - motion (D_{gm}) as follows,

$$\frac{y_{max}(f_{osc})}{y_{rms}(f_{osc})} = \sqrt{2}\int_0^{\infty}\{1-[1-\xi\exp(-z^2)]^{N_e}\}dz \quad (11)$$

where $$\xi(f_{osc}) = \frac{m_2}{\sqrt{m_0 m_4}}, \quad (12)$$

and the number of extrema N_e is given by

$$N_e(f_{osc}) = \frac{1}{\pi}\sqrt{\frac{m_4}{m_2}}\, D_{gm}. \quad (13)$$

The spectral moments (m_k, k=0, 2, 4) at each oscillator frequency are computed from the FAS of the response of a SDOF system, which is obtained by multiplying the FAS of the ground-motion with the instrument transfer function with 5% critical damping (equation (7), Bora et al., 2014). Therefore, in order to compute the D_{gm} corresponding to an acceleration trace, it is treated as a variable (in RVT based response spectrum) to minimize the misfit between the observed and RVT computed response spectrum. Essentially, a squared mismatch (in log space) is minimized at each oscillator-frequency. The required FAS for the RVT computed response spectrum is determined from the observed record. In the present study a different measure of duration (D_{rms}) was not used for computing the y_{rms}. Therefore the y_{rms} is computed by using the zeroth order spectral moment (m_0) and the D_{gm} as follows,

$$y_{rms}(f_{osc}) = \sqrt{\frac{m_0}{D_{gm}}} \quad (14)$$

The Figure 10 depicts plots of the determined D_{gm} against the oscillator-frequency for some representative scenarios of magnitude and distance. The panel on the right in Figure 10 depicts

the closeness of the RVT optimized and observed response spectrum. The D_{gm} was determined only for usable oscillator-frequencies corresponding to the observed response spectrum of the recorded acceleration trace. The useable oscillator frequency limits were decided as the 1.25 and 0.8 times of the cut-off frequencies of the corresponding filters at the low and high frequency ends of the Fourier spectra respectively. It is worth mentioning here that the D_{gm} values estimated in this way are consistent within the use of RVT framework and conditioned to the 5% critical damping of the SDOF system. Hence a care is suggested before comparing those values with the other measures of ground-motion duration. However, it is believed to represents a combination of several effects on here determined estimate of duration, D_{gm} including the effect of oscillator response along with the earthquake size, source-to-site distance and the local site condition effects. Although, the present estimate of duration is different than the estimate in Bora et al. (2014) in that it does not incorporate the use a different estimate of duration (i.e. D_{rms}) for computing y_{rms} (in its estimation), the notation D_{gm} is used for the present duration estimates.

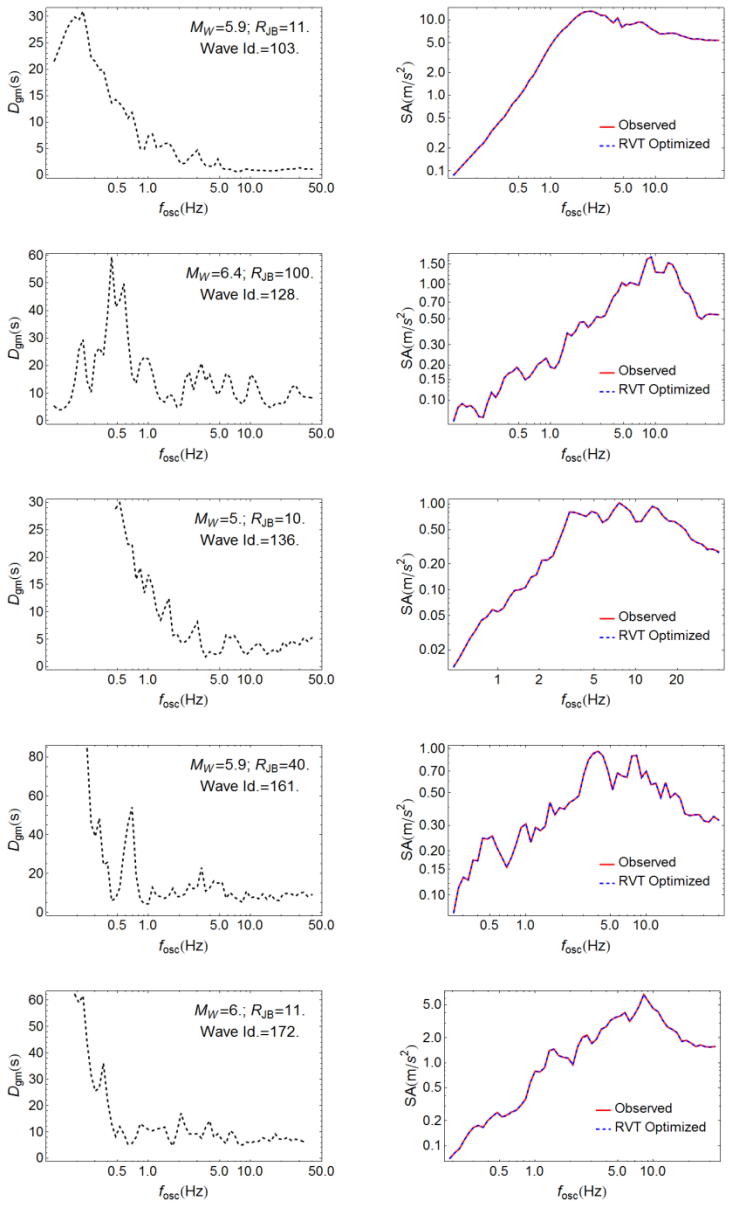

Figure 10 Left panels depict plot of duration (D_{gm}) against oscillator frequency for 5% critical damping. Right panels depict the corresponding match between observed and RVT optimized response spectra.

6.2 Regression model for duration (D_{gm})

A revised functional form for duration model is used in this study; to that effect an additive functional form is employed as opposed to the multiplicative form in Bora et al. (2014). However a test to check the effect of the duration-model functional form on the variance of the response spectral ordinates was performed. Both the additive and multiplicative forms were tested and no

significant difference was obtained in terms of the variance of the final response spectral ordinates. Similar to the FAS, a set of three empirical regression models are derived for D_{gm}. The functional form of the three regression models is as follows,

$$\ln D_{gm}(f_{osc}) = \ln[d_0 + d_1 M_W + d_2\sqrt{R_{JB}^2 + d_3^2} + d_4 Vs_{30}] \,, \quad (15)$$

$$\ln D_{gm}(f_{osc}) = \ln[d_0 + d_1 M_W + d_2\sqrt{R_{JB}^2 + d_3^2} + d_4 Vs_{30} + d_5\kappa], \quad (16)$$

and

$$\ln D_{gm}(f_{osc}) = \ln[d_0 + d_1 M_W + d_2\Delta\sigma + d_3\sqrt{R_{JB}^2 + d_4^2} + d_5 Vs_{30} + d_6\kappa]. \quad (17)$$

The functional form in equation (16) and (17) include $\Delta\sigma$ and κ as predictor variables in addition to M_W, R_{JB} and Vs_{30}. Inclusion of these additional parameters is motivated by the requirement of consistency with the earlier derived empirical FAS model which will allow making consistent adjustments to both the duration and FAS to reflect variations in $\Delta\sigma$ and κ. At present, it is difficult to say what the exact dependence of the D_{gm} over these parameters is supposed to be. However one can determine an empirical dependence using a simple functional form.

The regression was performed using equation (15), (16) and (17) at each oscillator-frequency in the range 0.2-21.93 Hz. The definition of predictor variables remains same as in equation (7), (8) and (9). The same random effects algorithm of Abrahamson and Youngs (1992) was performed to decompose the residuals in between- and within-event terms which are considered to be log-normally distributed with standard deviation τ and ϕ respectively. The total standard deviation

was computed using equation (10). Geometric mean of the duration from the two horizontal components was considered to perform the regression.

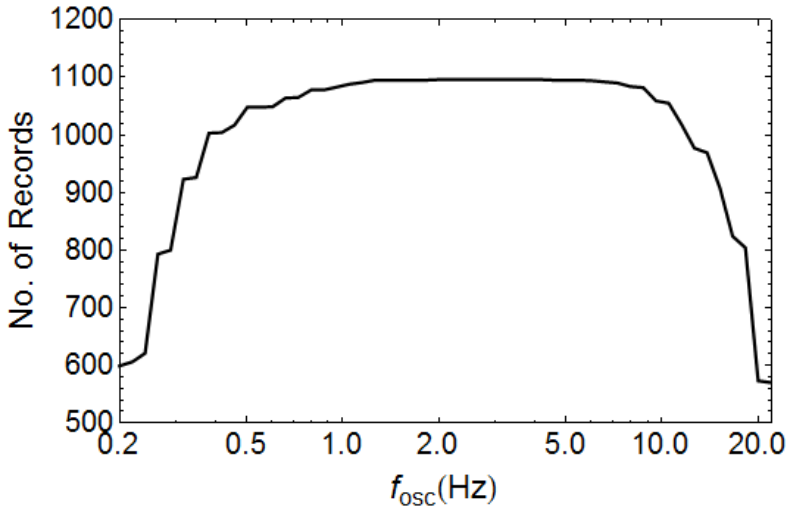

Figure 11 Variation of number of records with chosen oscillator frequencies for deriving empirical model for D_{gm}.

For having smoothed variation of the predicted D_{gm} with respect to oscillator frequency a smoothed D_{gm} value is chosen at a selected oscillator frequency. The earlier mentioned smoothing scheme for FAS is used to smooth the D_{gm} as well. The smoothened D_{gm} was selected at 52 oscillator frequency ordinates spanning in the range 0.2-21.93 Hz with log spacing of 0.04. However, the extent of smoothing should be such that the RVT optimized response spectrum should remain unchanged. In order to check this visually, the RVT based response spectrum was re-computed using the smoothed D_{gm} and compare it with the observed response spectrum. Due to the limited usable oscillator frequency range in observed response spectra and different usable frequency limits for each record the number of data points at all the oscillator frequencies were not the same. The variation of number of data points at each oscillator frequency is depicted in Figure 11. For obtaining a physical scaling of D_{gm} with respect to magnitude and distance a constrained regression was performed by forcing by forcing d_1 and d_3 to be positive. The values

of the coefficients involved in equation (15), (16) and (17) are listed in Table 4, Table 5 and Table 6 respectively. The Tables can be found in the appendix.

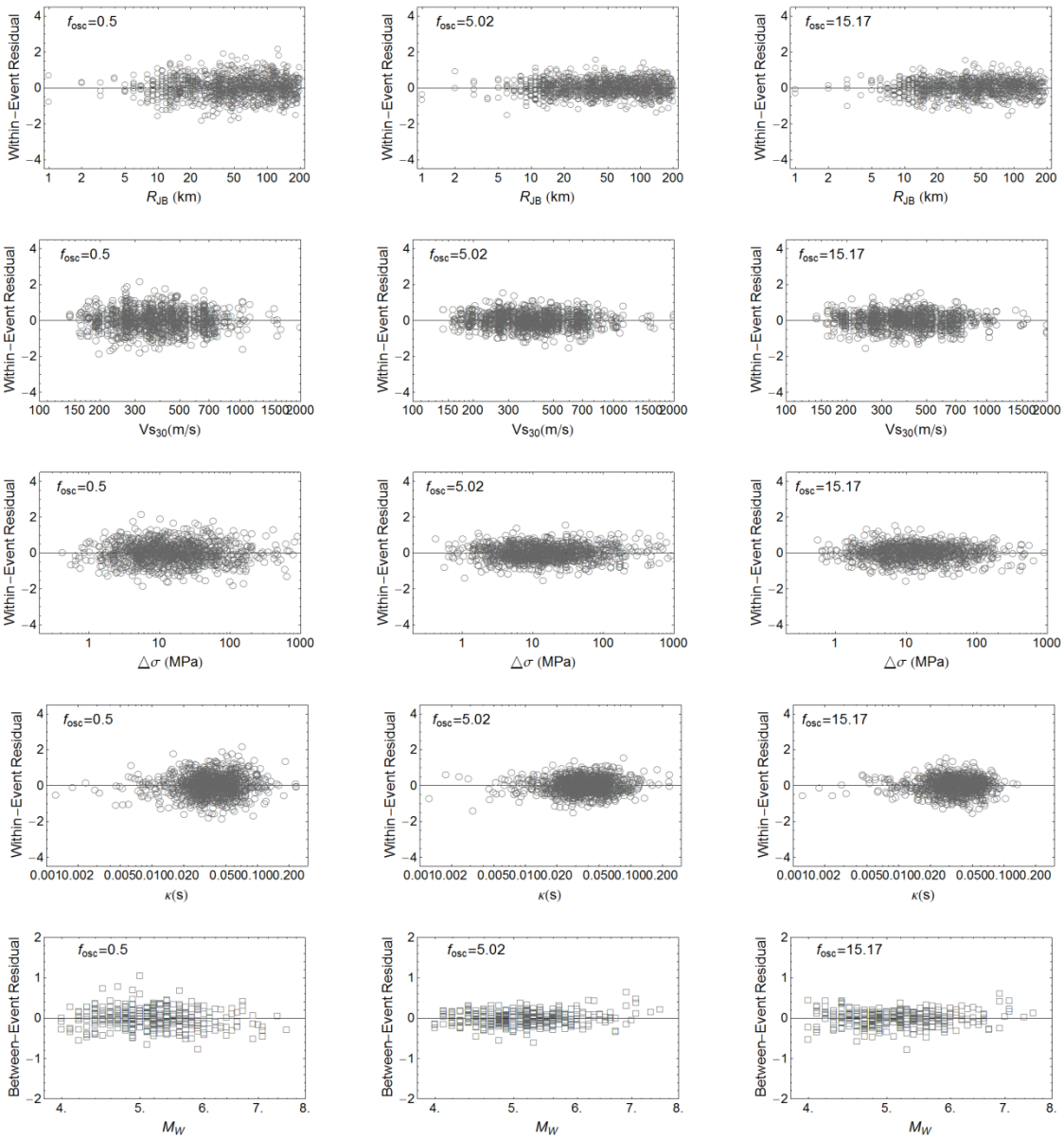

Figure 12 Plot of within-and between-event residuals corresponding to D_{gm} model against the five predictor variables (M_W, R_{JB}, Vs_{30}, Δσ and κ) at f_{osc}= 0.5, 5.02 and 15.17 Hz.

In order to check the robustness of the derived empirical models the residuals obtained from the regression of equation (17) are plotted against the five predictor variables. Figure 12 depicts the

plot of between-event residuals against magnitude, within-events residuals against distance, Vs_{30}, $\Delta\sigma$ and κ at f_{osc}= 0.5, 5.02 and 15.17 Hz. In general greater dispersion is observed at 0.5 Hz which gradually decreases at 5.02 and 15.17 Hz. The between-event residuals indicate larger spread at 0.5 Hz towards magnitudes M_W <5; a similar behavior can also be observed at 15.17 Hz.

Figure 13 depicts the variation of median D_{gm} with respect to oscillator-frequency corresponding to all the predictor variables (M_W, R_{JB}, Vs_{30}, $\Delta\sigma$ and κ) involved in equation (17). In Figure 13 the D_{gm} values are observed to be higher at low oscillator-frequencies and decreasing towards higher oscillator-frequencies. There can be several-effects that control such a behavior such as the effect of the oscillator response in which the damping of the oscillator can have strong influence. However, for the critical damping that is used in this study (i.e. 5%) it can also be observed that seismological parameters like earthquake size, source-to-site distance also influence the D_{gm} being strongest at low oscillator-frequencies. The parameter Vs_{30} is found to affect the D_{gm} estimates only at low oscillator-frequencies. A similar influence is observed for record-specific $\Delta\sigma$ and κ parameters.

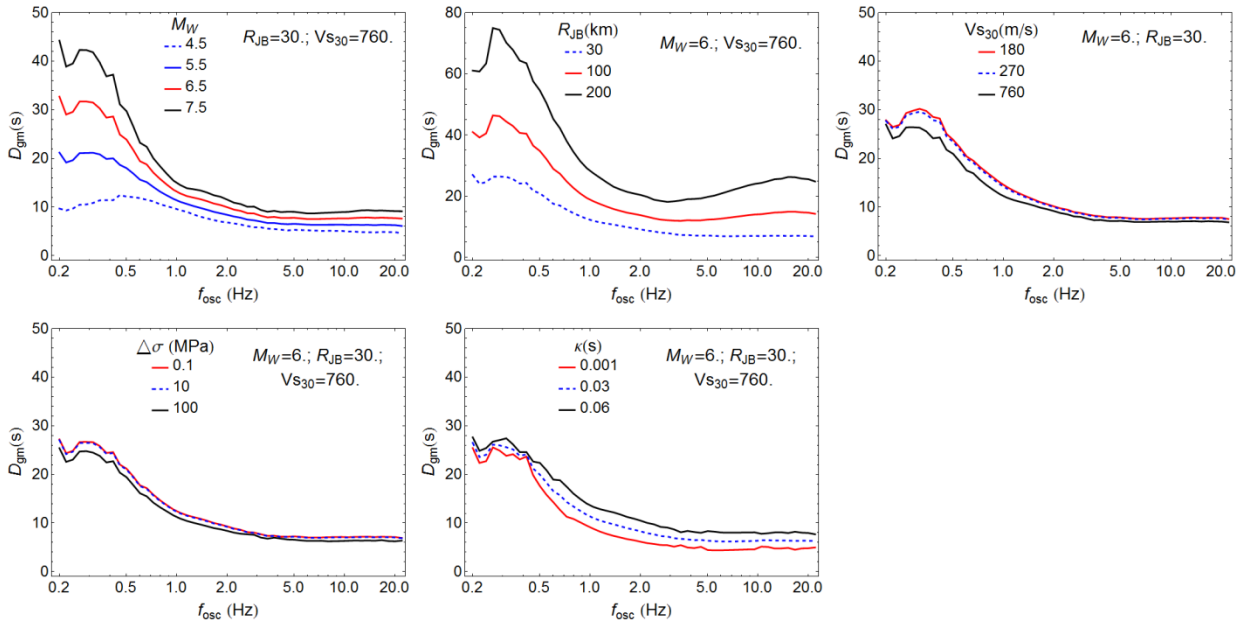

Figure 13 Variation of predicted duration against the oscillator-frequency for different scenarios of magnitude, distance, Vs_{30}, $\Delta\sigma$ and κ.

7. Response spectra

As mentioned earlier, in this study the response spectrum is computed using a combination of the empirical FAS model and the empirical duration model. Essentially, equations (11-14) are used to obtain the forward predictions of the response spectra using the two empirical models of FAS and D_{gm}. As noted earlier, the empirical duration model is derived for the oscillator frequencies in the range 0.2-21.93 Hz. For having the D_{gm} estimates at f_{osc}<0.21 and f_{osc}>21.93 Hz the values corresponding to 0.21 and 21.93 Hz are considered respectively. In order to obtain the final median response spectral ordinates four combinations of predicted FAS and D_{gm} were tested in terms of mean and median values. The conversion from median to mean of Fourier spectral amplitudes assumes a lognormal distribution at each frequency ordinate. The Fourier spectral amplitudes at different frequencies can not be considered as independent to one another. However, it was observed that the combination of mean FAS and mean D_{gm} values gives the best estimate of median predicted response spectra in terms of variance. Hence, in order to obtain the

median response spectral presented in this study the mean values of both FAS and D_{gm} predictions are used.

For having a consistency check, a comparison is performed, in terms of median predictions, between the presented analysis and other GMPEs which have been developed using the same database (RESORCE). Only the GMPEs of Akkar et al. (2014), Bindi et al. (2014) and Bora et al. (2014) are considered for comparison as they involve a parametric functional form in their regression analysis. Comparison amongst the median GMPEs was performed for the same scenarios of magnitude, distance and Vs_{30} which have been used in Douglas et al. (2014). However, for having a consistency between Fourier spectrum and response spectrum the use of oscillator-frequency ordinate is preferred as opposed to the periods used by Douglas et al. (2014). In passing it is worth noting that of Douglas et al. (2014) uses the comparison paper of Abrahamson et al., (2008) as the template; hence comparison between the figures presented here can also be made to those shown in Abrahamson et al. (2008). Moreover, the GMPE of Boore et al. (2013) is also used which is expected to facilitate a comparison between the presented approach and NGA (Next Generation Attenuation) models. This NGA model was chosen because it utilizes R_{JB} as the distance metric.

7.1 Distance scaling

The attenuation with distance for PGA and 1 Hz spectral amplitude with critical damping 5% is presented in Figure 14. Figure 14 depicts the comparison for Vs_{30} =760 m/s and Figure 15 depicts the same comparison for Vs_{30}=270 m/s. It is to be noted that 100 Hz spectral amplitude is considered as the PGA in the present approach. The D_{gm} estimate at f_{osc}=21.93 Hz is used to make the prediction at f_{osc}=100 Hz. The dataset selected in the present study for deriving the GMPEs does not contain any earthquake beyond magnitude 7.6. Nevertheless, for having

consistency in comparing the predictions with the other GMPEs, predictions from presented approach are shown for M_W=8. The shape of the distance scaling presented in this study is similar to the other models considered here. A slower decay rate with distance can be observed towards the larger magnitude. For PGA, the decay rate predicted by the present approach is observed to be similar to the decay rate predicted by Akkar et al. (2014) and Bindi et al. (2014); however it is faster than predicted by Boore et al. (2013). For the 1 Hz spectral amplitude, present approach predicts a slightly slower decay rate in comparison to the other two RESORCE GMPEs.

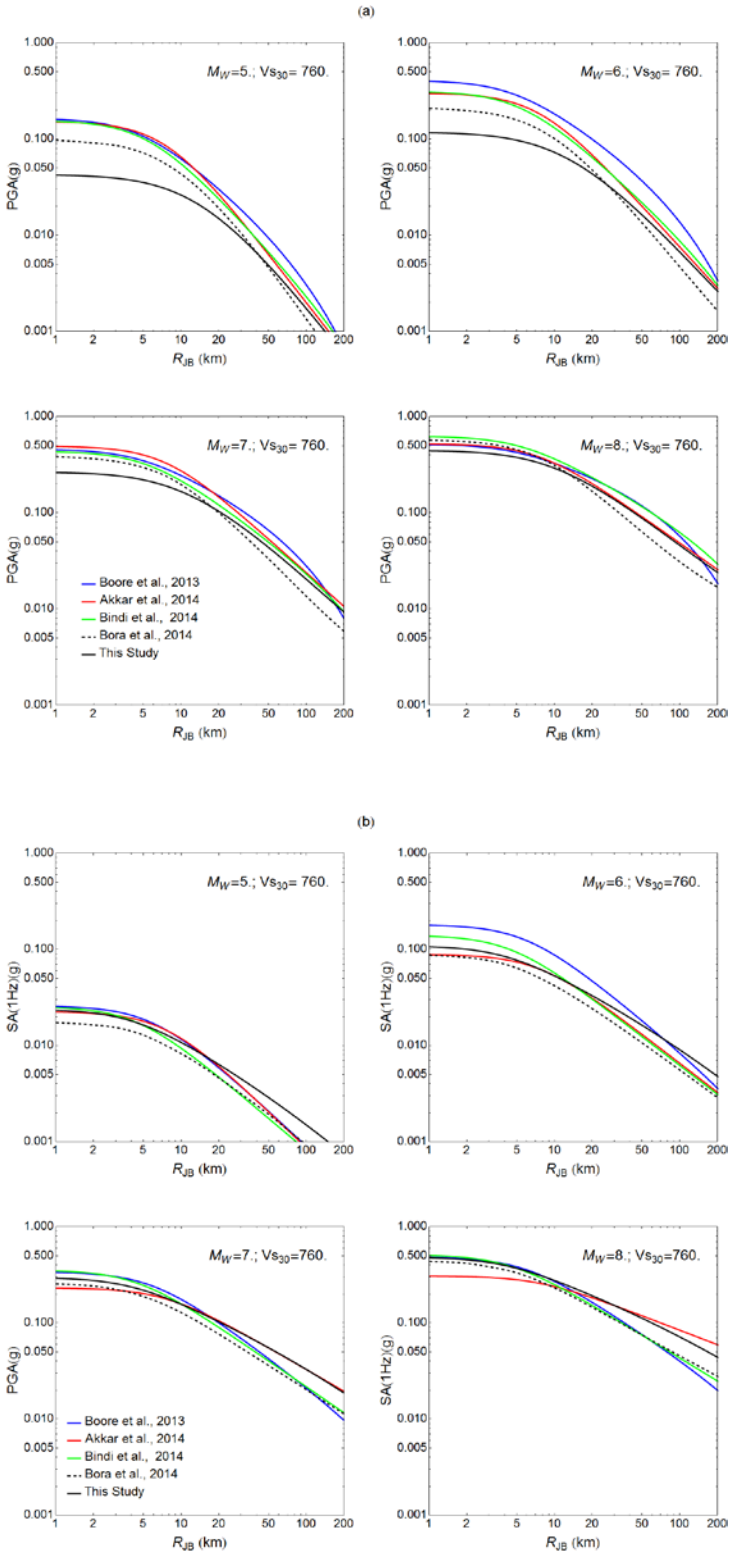

Figure 14 Comparison of distance scaling for strike-slip earthquakes corresponding to Vs_{30}=760 m/s (a) PGA (b) SA at f_{osc} =1 Hz. Predictions from present model are obtained for $\Delta\sigma$=14.5 MPa and κ_0=0.042 s.

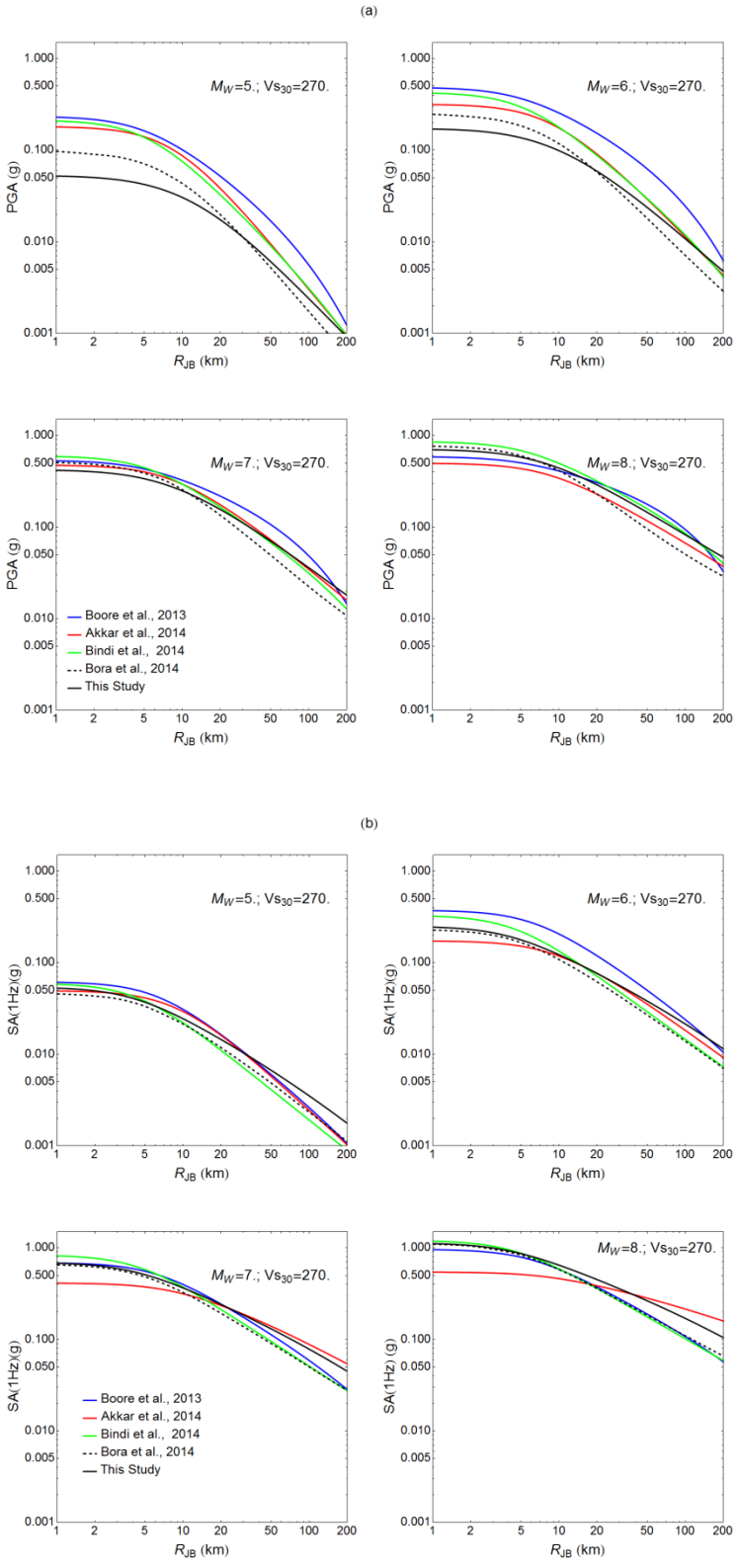

Figure 15 Comparison of distance scaling for strike-slip earthquakes corresponding to Vs_{30}=270 m/s (a) PGA (b) SA at f_{osc} =1 Hz. Predictions from present model are obtained for $\Delta\sigma$=14.5 MPa and κ_0=0.042 s.

7.2 Magnitude scaling

Scaling of PGA and spectral amplitudes at f_{osc}= 0.33, 1, and 5 Hz is shown in Figure 16. The ordering of the panels in this figure is kept in increasing order of response period in order to maintain consistency with Douglas et al. (2014). The nonlinear magnitude scaling of spectral amplitudes with larger magnitude is readily visible. Overall, the magnitude scaling obtained from present approach is seen to be in good agreement with that from other GMPEs.

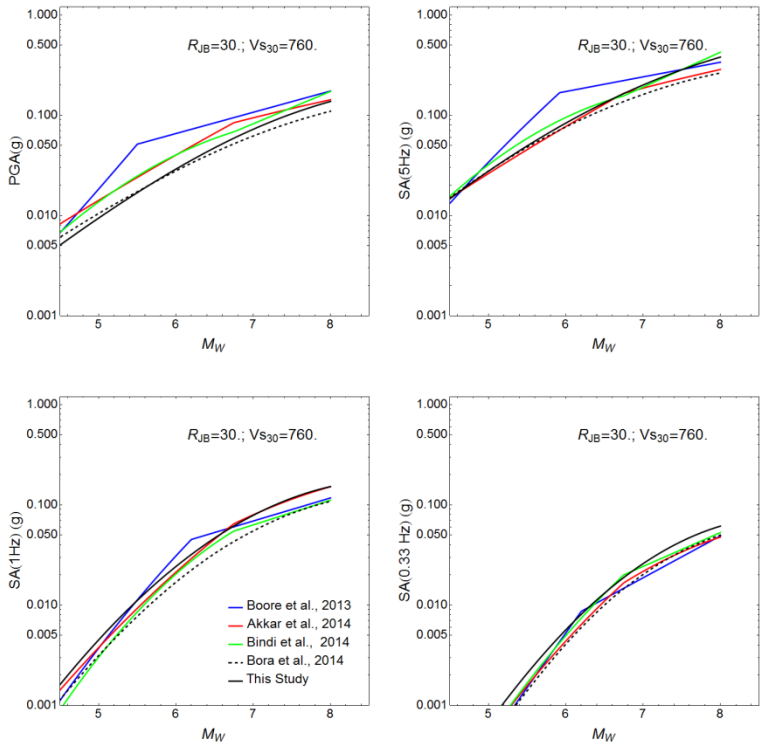

Figure 16 Comparison of magnitude scaling of median predicted PGA (top left) and response spectral ordinates for strike-slip earthquakes at f_{osc}= 5 Hz (top right), 1 Hz (bottom left) and 0.33 Hz (bottom right) corresponding to Vs_{30} =760 m/s. Predictions from present model are obtained for $\Delta\sigma$=14.5 MPa and κ_0=0.042 s.

The PGA values predicted from the present study and those by Akkar et al. (2014) and Bindi et al. (2014) are observed to be similar. However towards low oscillator frequencies the values presented from present approach are slightly higher at f_{osc}=0.3 and 1 Hz. The median values of

$\Delta\sigma$=14.5 MPa and similarly a mean κ_0=0.042 are used for obtaining the response spectra using the approach presented herein.

7.3 Scaling with Vs_{30}

The scaling of response spectral ordinates with Vs_{30} is depicted in Figure 17. The models presented in this study do not account for any nonlinear site behavior given that the majority of the recordings in the dataset correspond to low-to-moderate earthquake magnitudes, which are not expected to produce strong nonlinear effects. However, the broad trend that can be observed from Figure 17 is that the low Vs_{30} values give rise to higher spectral amplitudes and vice-versa. It can be easily observed from figure 17 a and b that the scaling of response spectral ordinates with Vs_{30} predicted from the present study indicates an overall good agreement with the other RESORCE GMPEs at both R_{JB}=100 and 10 km. Figure 18 shows the variation of the ratio of spectral amplitudes on sites with Vs_{30} of 270 and 760m/s at different oscillator frequencies for two different distances of R_{JB}=10 and 100 km (left panels) and for sites with V_{s30} values of 490 and 760m/s in the panels on the right. Figure 18 also depicts that the ratio of spectral amplitudes predicted from the present study are found to be in good agreement with those obtained from other RESORCE GMPEs including the model of Boore et al. (2013).

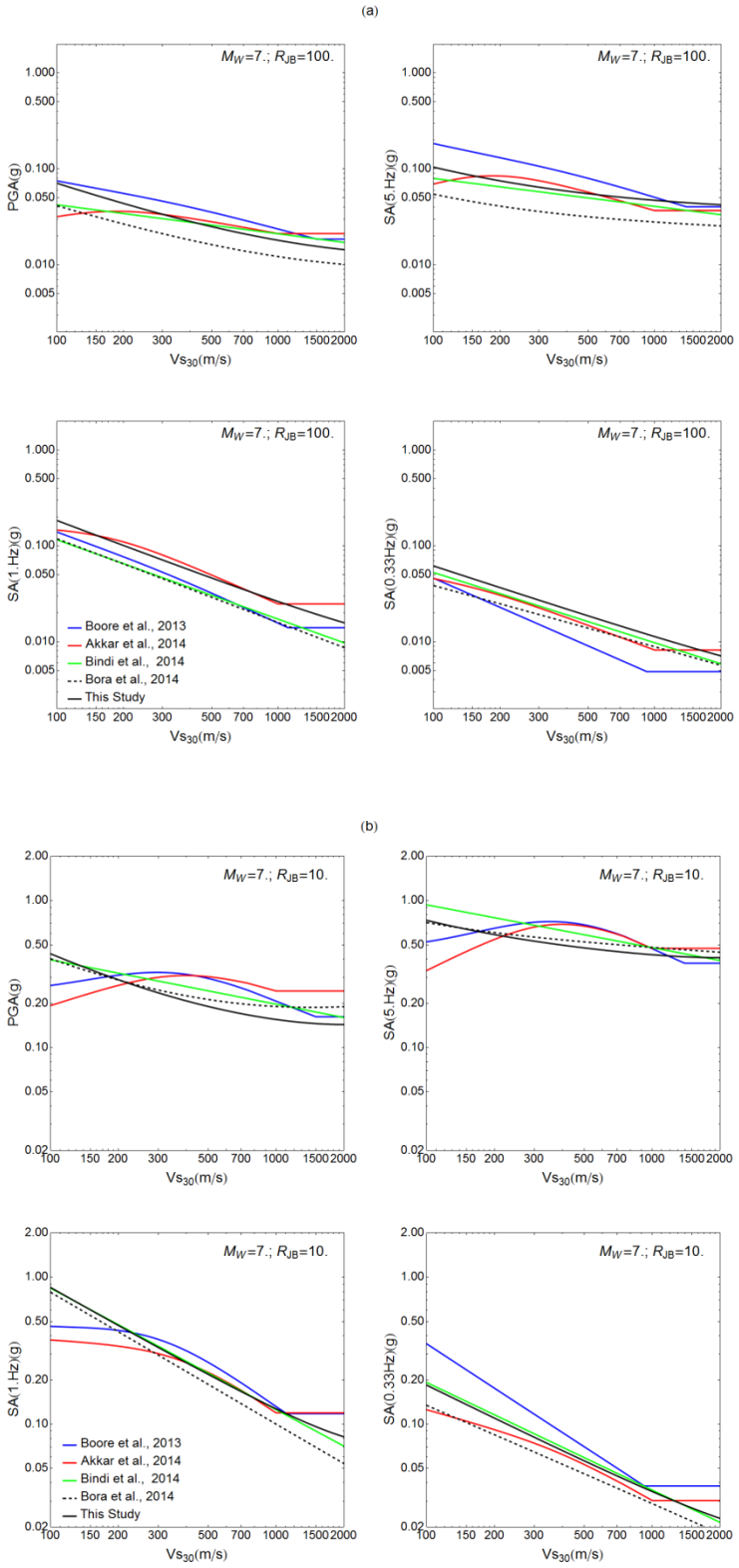

Figure 17 Comparison of Vs_{30} scaling of the median ground motion for strike-slip earthquake with M_W 7 for PGA and response spectral ordinates at f_{osc}= 5 Hz (top right), 1 Hz (bottom left) and 0.33 Hz (bottom right) at R_{JB}= 100 km (a) and R_{JB}=10 km (b). Predictions from present model are obtained for $\Delta\sigma$=14.5 MPa and κ_0=0.042 s.

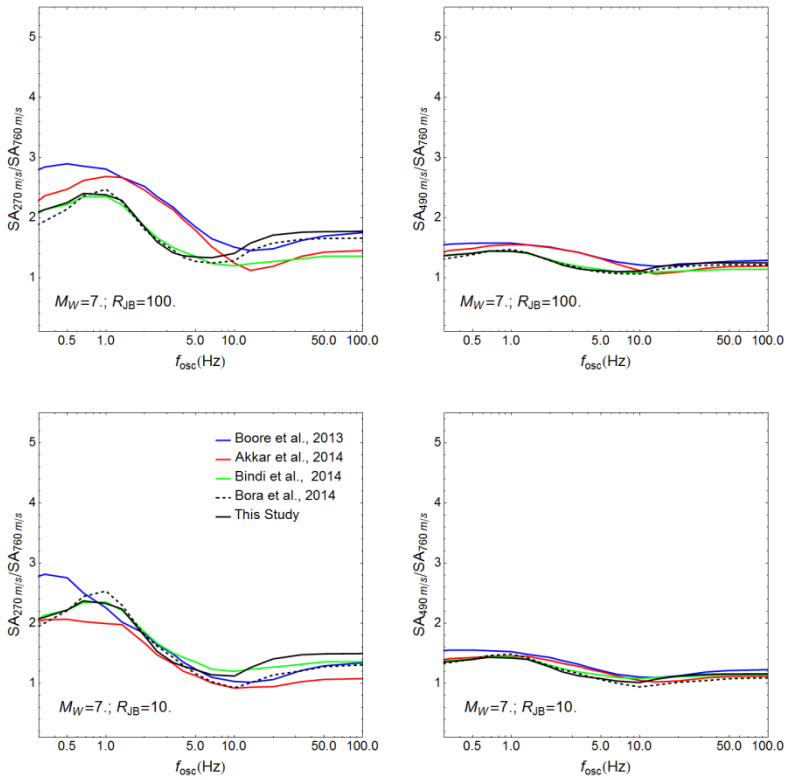

Figure 18 Comparison of ratios between SA for Vs_{30}=270 m/s (left) and SA for Vs_{30}=490 m/s (right) to SA for Vs_{30}=760 m/s for strike-slip earthquake M_W 7 at R_{JB}=100 km (top) and R_{JB}=10 km (bottom). Predictions from present model are obtained for $\Delta\sigma$=14.5 MPa and κ_0=0.042 s.

7.4 Predicted response spectra

Predicted response spectra for M_W=5, 6, 7 and 8 at R_{JB}=10 km corresponding to Vs_{30}=760 m/s are depicted in Figure 19. In general the response spectral values obtained by present approach are seen to be in good agreement with the other models at low oscillator frequencies but predict lower amplitudes at high frequencies. For M_W=7 the overall spectrum from this approach is found to be very comparable with the other models. The lower spectral amplitudes at high oscillator-frequencies can be attributed to the relatively higher κ value used for prediction which may not be a representative for other GMPEs. Figure 20 depicts, the response spectra for M_W=7 at R_{JB}=10 km corresponding to Vs_{30}=270 and 760 m/s. The values from present model for low Vs_{30} values are seen to be generally in good agreement with the other models, but are slightly

higher at low oscillator frequencies. Similar behavior is observed for the stiffer site, although at high frequencies the predictions of presented new model amongst the lowest.

Additionally, the scaling of response spectra with Δσ and κ is depicted in Figure 21. The left panel depicts the Δσ scaling of response spectra for different magnitudes corresponding to Vs_{30}=760 m/s. The Δσ is observed to affect the high oscillator-frequency amplitudes, increasing the spectral level with increasing Δσ. The low oscillator frequency spectral amplitudes are almost unaffected by the change in the Δσ which are completely determined by the magnitude. The left panel in Figure 21 depicts the scaling with respect to κ for different Δσ values. It can easily be seen that the high-frequency response spectral amplitudes are completely determined by the Δσ and κ for a fixed magnitude, distance and Vs_{30} scenario. The Δσ is seen to affect the spectral amplitudes at frequencies > 0.3 Hz whereas κ influences the spectral amplitudes beyond 2 Hz.

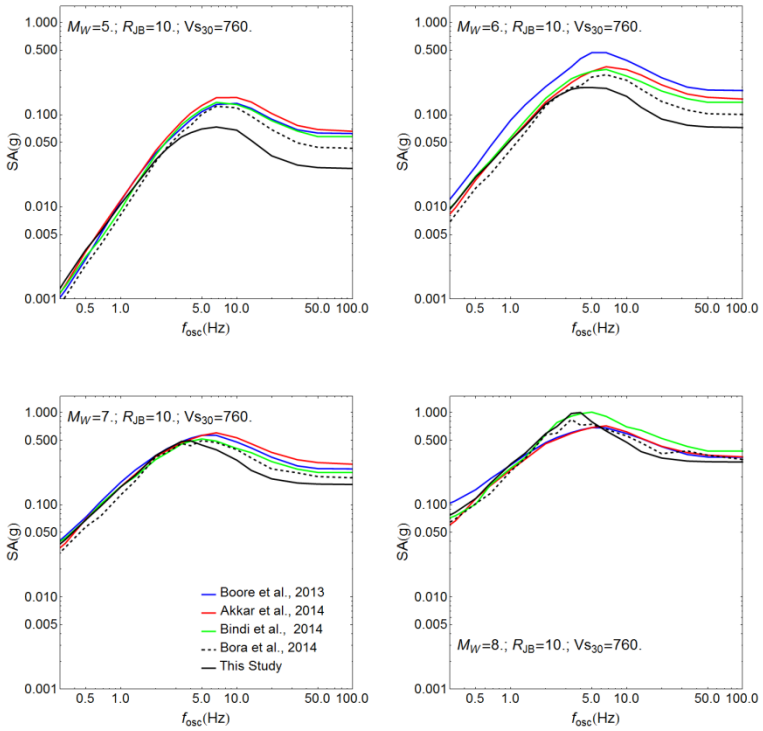

Figure 19 Comparison of median predicted response spectra for strike-slip earthquakes corresponding to Vs_{30}=760 m/s at R_{JB}=10 km. Predictions from present model are obtained for Δσ=14.5 MPa and κ_0=0.042 s.

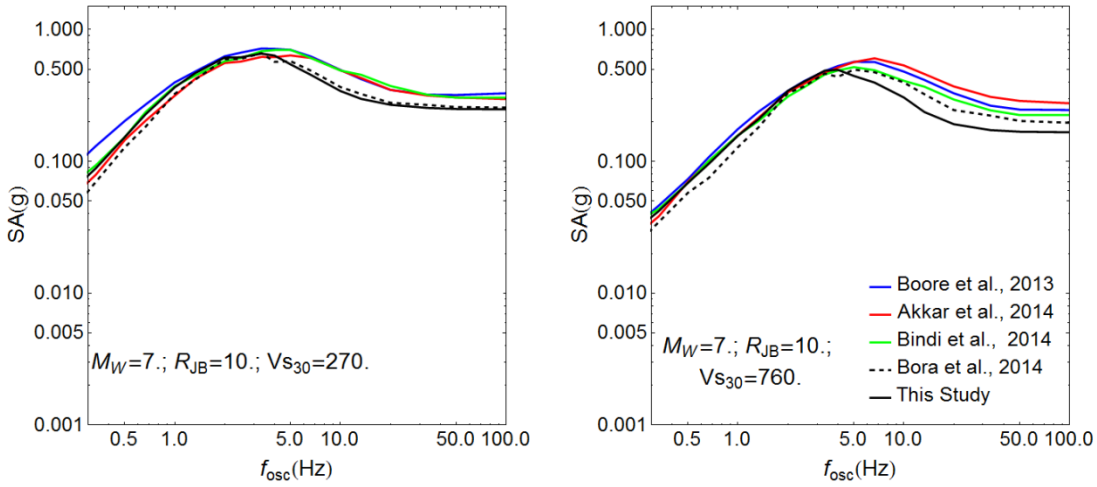

Figure 20 Comparison of median predicted response spectra for strike slip earthquake M_W=7 corresponding to Vs_{30}=270 m/s (left) and Vs_{30}=760 m/s (right) at R_{JB}=10 km. Predictions from present model are obtained for $\Delta\sigma$=14.5 MPa and κ_0=0.042 s.

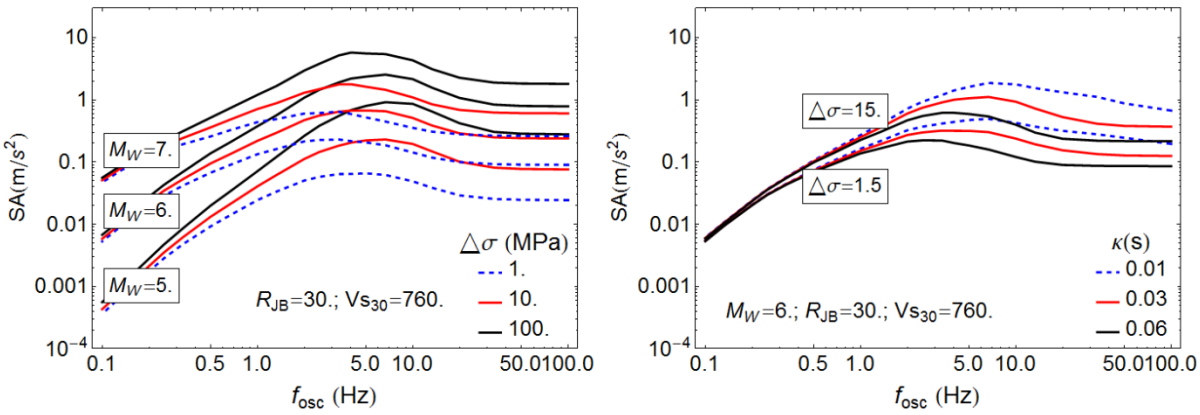

Figure 21 Scaling of response spectra with stress parameter (left) for M_W 5 , 6 and 7 corresponding to Vs_{30}=760 m/s. Right panel depicts the scaling of response spectra for M_W 6 with κ corresponding to $\Delta\sigma$=1.5 and 15 MPa.

7.5 Variability in response spectra

Finally, an estimate of the aleatory uncertainty involved in the predicted response spectra using the present analysis is performed. For the purpose, the response spectral residuals are computed and for obtaining the residuals at each oscillator frequency the log (natural) of the predicted spectral amplitudes are subtracted from the log (natural) of the observed corresponding spectral

amplitudes. The predicted spectral amplitudes are obtained by combining the predictions from FAS and duration models through RVT. Subsequently, the residuals are partitioned in to between-event and within-event components using the algorithm suggested by Abrahamson and Youngs (1992). In Figure 22, both the residuals at f_{osc}=0.3, 5 and 100 Hz are plotted against all the five predictor variables used in empirical models for FAS and duration. Although, the residuals have not been computed as the outcome of a standard regression procedure, a stable variation of the residuals around zero can be observed. The scatter amongst the residuals is seen larger towards the low oscillator-frequency in comparison to the high frequencies. For between-event residuals the scatter is seen larger at f_{osc}=0.3 Hz and a slight over prediction is also observed. A similar trend was observed by Bindi et al. (2014) which they attribute to the unfiltered noise present for some low magnitude events. Although, the style-of-faulting was not included as the predictor variable in the empirical models presented in this study for FAS and $D_{gm,}$ the residuals are depicted for the three styles of faulting in Figure 23. Over all there is no trend observed except for the normal faulting at f_{osc}=100 Hz.

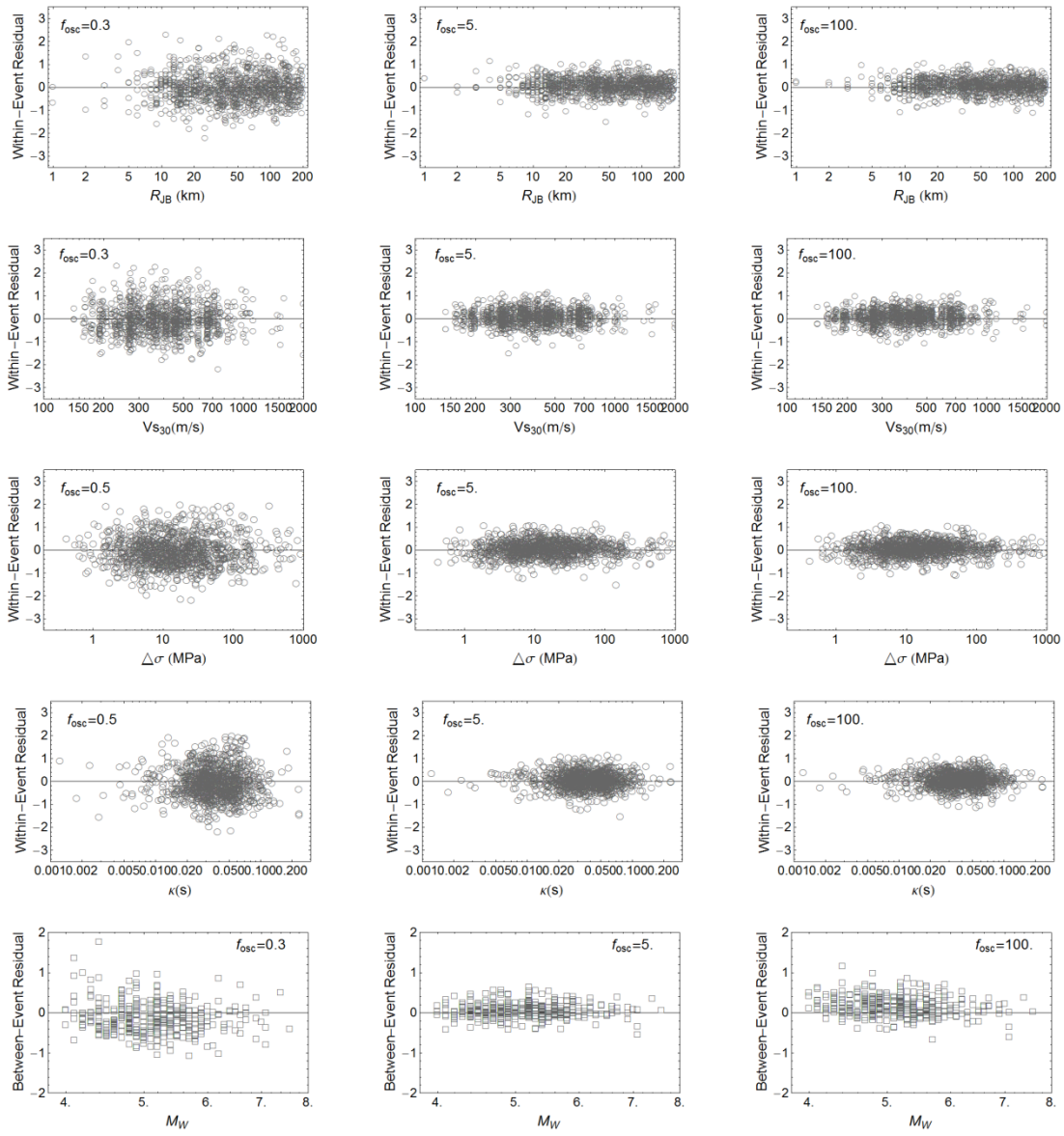

Figure 22 Plots of within (circles)-and between-event (squares) response spectral residuals against M_W, R_{JB}, Vs_{30}, $\Delta\sigma$ and κ at f_{osc} = 0.5, 5 and 100 Hz.

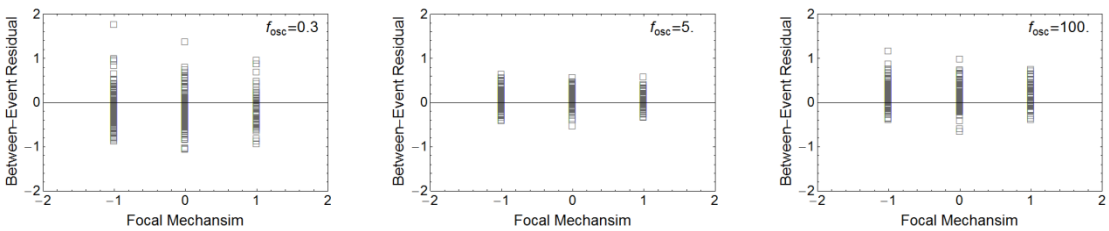

Figure 23 Plots depicting the variation of between-event residuals with the respect to the style-of-faulting where -1, 0 and 1 represent normal, strike-slip and reverse faulting respectively.

Figure 24 depicts the variation of aleatory variability in terms of between-event (τ), within-event (ϕ) and total (σ) standard deviation against oscillator-frequency respectively. For comparison in Figure 24 the τ_2, ϕ_2 and σ values of Boore et al. (2013) are used. One of the technical hurdles associated with the earlier presented model in Bora et al. (2014) was the high values of total standard deviation. One of the notable achievements of this study that can be observed in Figure 24 is that a significant reduction in all three standard deviation values is obtained at high oscillator frequencies. The most striking feature that can be observed is the total standard deviation beyond f_{osc}=2.5 are lower by a factor of two in comparison to the models of Akkar et al. (2014) and Bindi et al. (2014). The values of the within-event standard deviation (and hence the total standard deviation) are also found to be lower than those of Boore et al. (2013) at high frequencies. However, major part of this reduction obtained in the standard deviation can also be due to the approach presented herein for the development of response spectral GMPE in which the record specific $\Delta\sigma$ and κ parameters are used. Assuming that, this reduction in variability obtained by the approach presented herein may not reflect the true variability for usually given scenarios of event-specific $\Delta\sigma$ and station-specific κ parameter, the residuals were also computed using the event-specific $\Delta\sigma$ and station-specific κ parameter. The event-specific $\Delta\sigma$ was computed by averaging it over all the records originated from the given earthquake; similarly station-specific κ was determined by averaging it over all the record obtained at a given station. In addition to that, the database average values of $\Delta\sigma$ (median=14.5 MPa) and κ (mean=0.42s) parameter were also used to compute the residuals. Figure 25 depicts the variation, of τ, ϕ and σ for these two cases, with respect to oscillator-frequency along with the comparison with those of Akkar et al. (2014) GMPE.

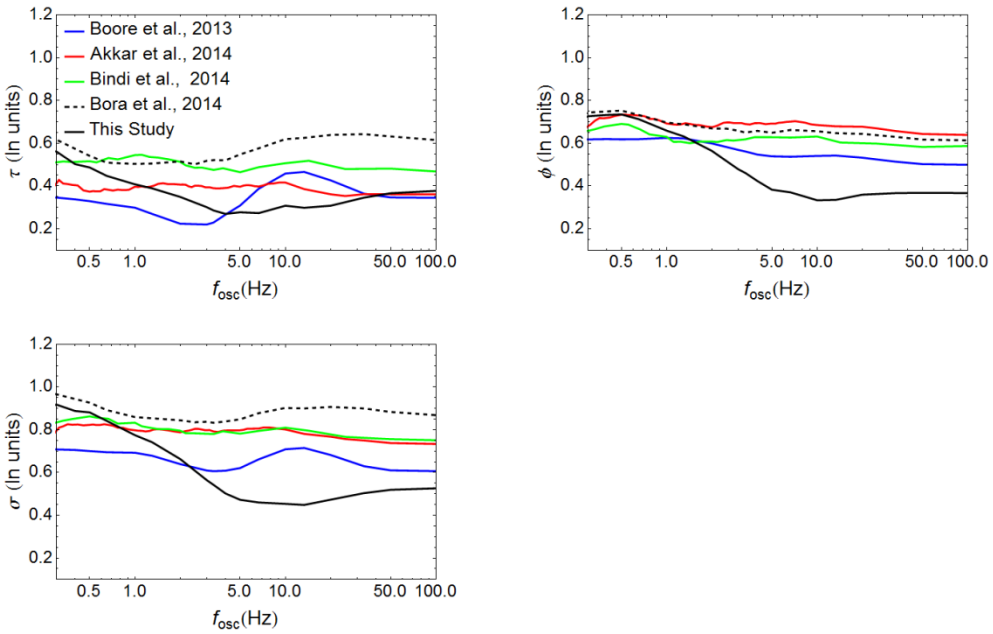

Figure 24 Comparison amongst the five models in-terms of between-event (τ), within-event (ϕ) and total standard deviation (σ).

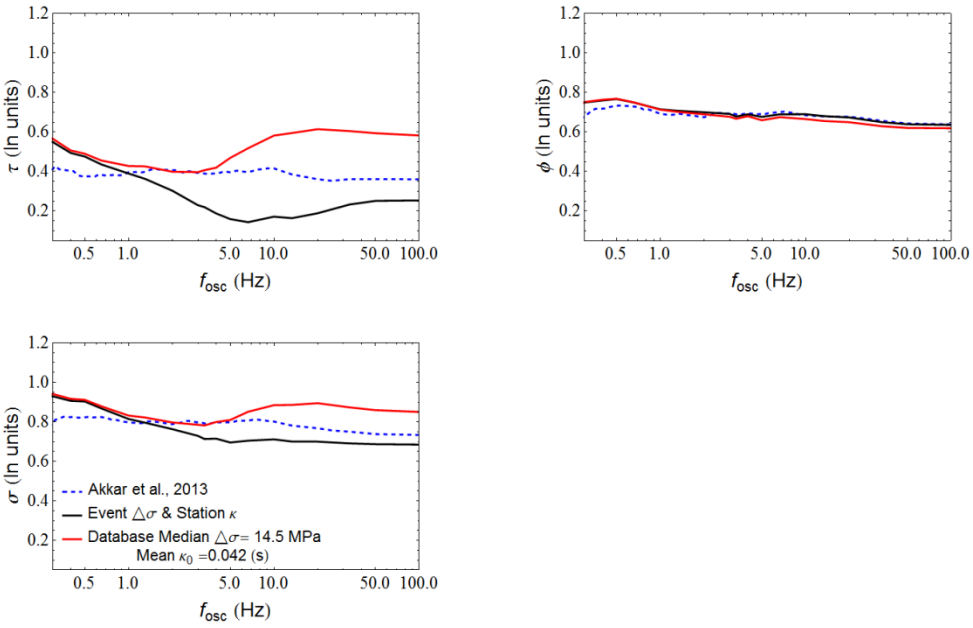

Figure 25 Plots depicting the variation of τ, ϕ and σ for the average values of Δσ and κ parameter.

Although the τ and σ values with the database-average values of $\Delta\sigma$ and κ parameter are seen higher than those of Akkar et al. (2014), the corresponding values are seen considerably lower with the event-specific and station-specific values of $\Delta\sigma$ and κ parameter.

8. Guidelines for using the present GMPE

As mentioned earlier, presented approach of developing a response spectral GMPE that provides options for adjusting the response spectral ordinates to different seismological conditions, is derived using the two separate empirical models for FAS and duration of ground-motion combined within the RVT framework. Based upon the method that is used to develop the present method of deriving a response spectral GMPE, certain guidelines are suggested for using the results presented in this document. As noted previously, the peak-factor of Cartwright, and Longuet-Higgins (1956) was used to relate the y_{max} and y_{rms}. A different definition of this peak-factor is expected to affect the estimates of D_{gm} from an observed accelerogram, likewise for making forward prediction of response spectra using the two empirical models. Hence for having a consistent estimate of response spectral ordinates the use of the same peak-factor is suggested. In addition to that, present analysis does not account for the oscillator effect on the input ground-motion duration to compute y_{rms}. This requires the assumption i.e. $D_{rms}=D_{gm}$ for making forward prediction for response spectra. Moreover, the D_{gm} estimates are determined for 5% critical damping of the SDOF system; consequently the empirical D_{gm} model derived herein should be considered valid with 5% critical damping of the oscillator. The low values of aleatory variability obtained are consistent with the methodological framework presented in this study. That has indicated that one will obtain a significant reduction in the aleatory provided the methodology presented herein is used. For scenarios, event-specific $\Delta\sigma$ and κ parameter or database-averaged values of these parameters the values of the total standard deviation given in Figure 25 should be

used. In addition to that, as mentioned previously that the results presented in this study are obtained for the mean values of predicted FAS and D_{gm}. Although Fourier spectral amplitudes are often considered as correlated, this decision was based upon the low values of variance (of median response spectra) obtained for this combination. However, it should be decided by the user that which values should be used.

9. Application of the present approach

As stated earlier, the ultimate aim of the present approach is to address the adjustability issues associated with the response spectral GMPE. The approach for developing a response spectral GMPE presented in this study provides options to make host-to-target adjustments in terms of different seismological parameters such as $\Delta\sigma$, site amplification and κ. additionally, the presented approach can be used to determine the host-to-target adjustment factors to be applied with the other existing response spectral GMPEs developed over the same database. In this section the two applications of the presented approach namely, 1) host-to-target adjustments with the presented GMPE and 2) generation of host-to-target adjustment factors are discussed. However the host-to-target adjustments are presented here in terms of the site condition effects.

9.1 Vs-κ adjustments

An application of the present approach for performing such host-to-target adjustments in terms of site effects is performed. For the purpose, two given target sites namely 1-V and 2-G are considered. The parameters associated with the two test sites are summarized in Table 7. The adjustments are performed at the rock level that is assumed to be underlying beneath the soil column.

Table 7

Site	Geometry	Thickness of the soil profile	Vs_{30} (surface)	Vs of target bedrock	Target κ (s)
1-V	1D	183 m	185 m/s	1500 m/s	0.03
2-G	1D/2D	690 m	370 m/s	3200 m/s	0.01

As discussed previously, the target adjustments can be easily performed with the presented approach. The procedure for applying the host-to-target corrections in terms of the rock amplification with the presented approach is straightforward as it involves four steps, 1) correction for the host rock amplification by dividing the median FAS by the respective rock amplification, 2) adjusting the corrected median FAS to the target rock amplification by multiplying the two, 4) adjustment related to κ can be obtained by using the corresponding values in the median FAS prediction equation i.e. equation (9), 5) adjustments in the duration estimates i.e. D_{gm} can be performed by using the respective target values of Vs_{30} and κ in the median prediction equation (17). Finally the target-adjusted median FAS and median D_{gm} are converted to the respective mean values before combining them within the RVT framework to obtain the target adjusted response spectra. It is to be noted that the empirical equations (9) and (17) are used to obtain the median FAS and D_{gm} respectively.

As stated earlier, the California rock velocity-profile anchored to Vs_{30}=620 m/s (Boore and Joyner, 1997) is assumed to be the reference rock profile for the empirical models presented in this study. Hence, the median predicted FAS is first corrected for this reference before applying the target rock profiles. A velocity profile corresponding to Vs_{30}=1500 m/s is considered for 1-V site, this profile is computed using the approach of (Cotton et al., 2006). For 2-G site the rock

profile corresponding to Eastern North America (Boore and Joyner, 1997) is considered; which is obtained by clipping-off the shallower part of the profile such that the shear-wave velocity becomes Vs=3200 m/s at the top of the rock. The rock-velocity profiles corresponding to the host and the two given target sites, used in the following analysis are depicted in Figure 26.

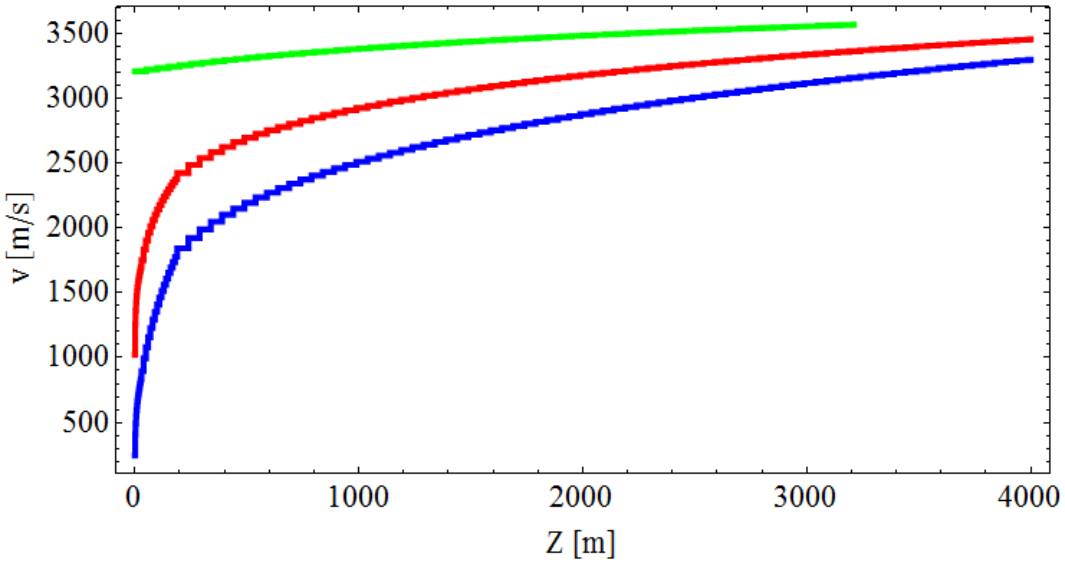

Figure 26 Plot depicting the velocity profiles which are used in the present host-to-target adjustments. The blue curve depicts the host profile corresponding to the California profile anchored at Vs_{30}=620 m/s; red curve depicts the target profile corresponding to site 1-V i.e. Vs30=1500 m/s and the green curve depicts the target profile for 2-G site i.e. Vs=3200 m/s.

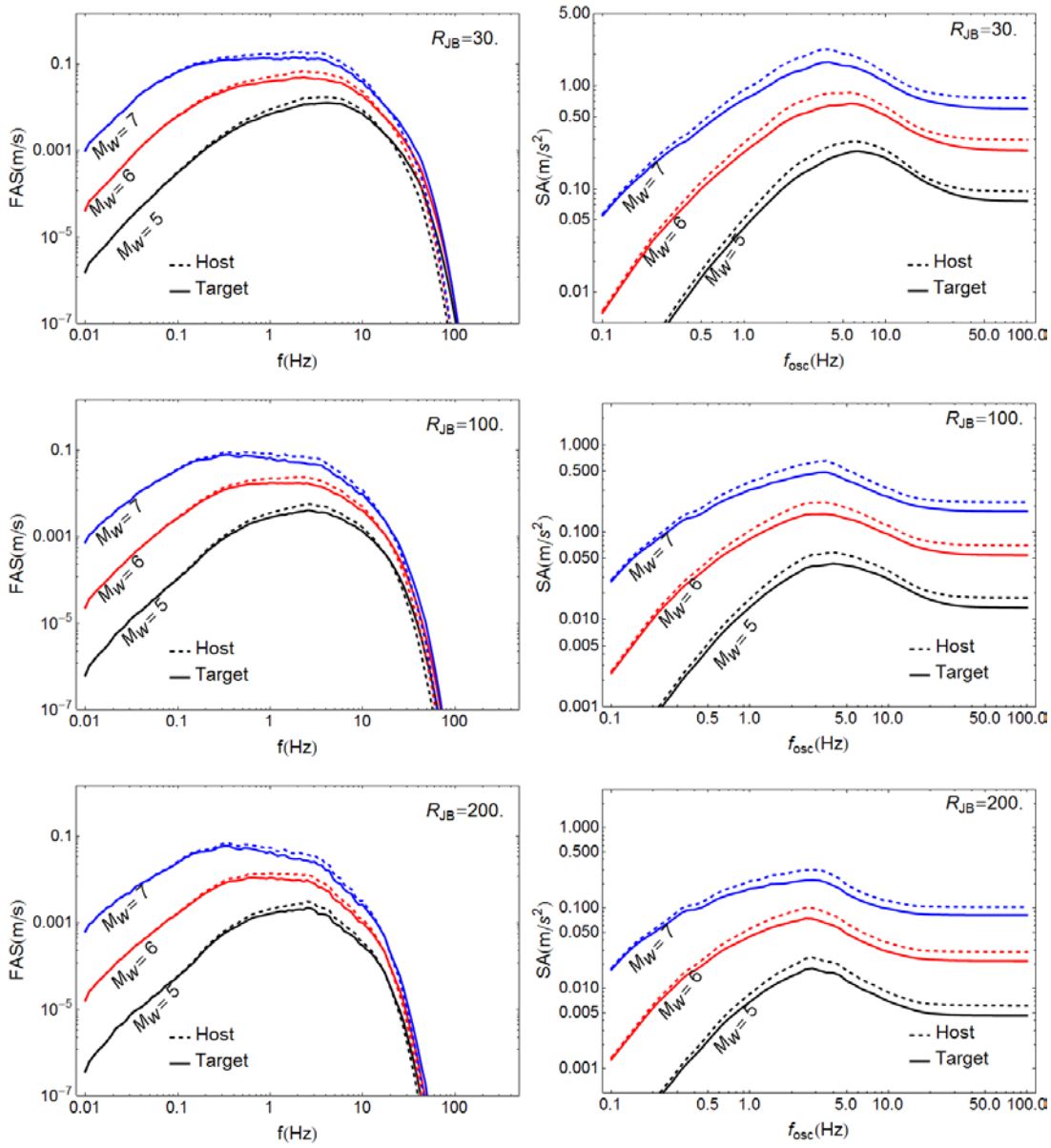

Figure 27 Plot depicting the host and target FAS (left) and corresponding response spectra (right) for the given test site 1-V. The host predictions are obtained for $\Delta\sigma$=14.5 MPa, Vs_{30}=620 m/s and κ=0.042 (s).

The amplification functions corresponding to those rock profiles were computed using the quarter-wavelength approach as suggested by (Boore and Joyner, 1997).

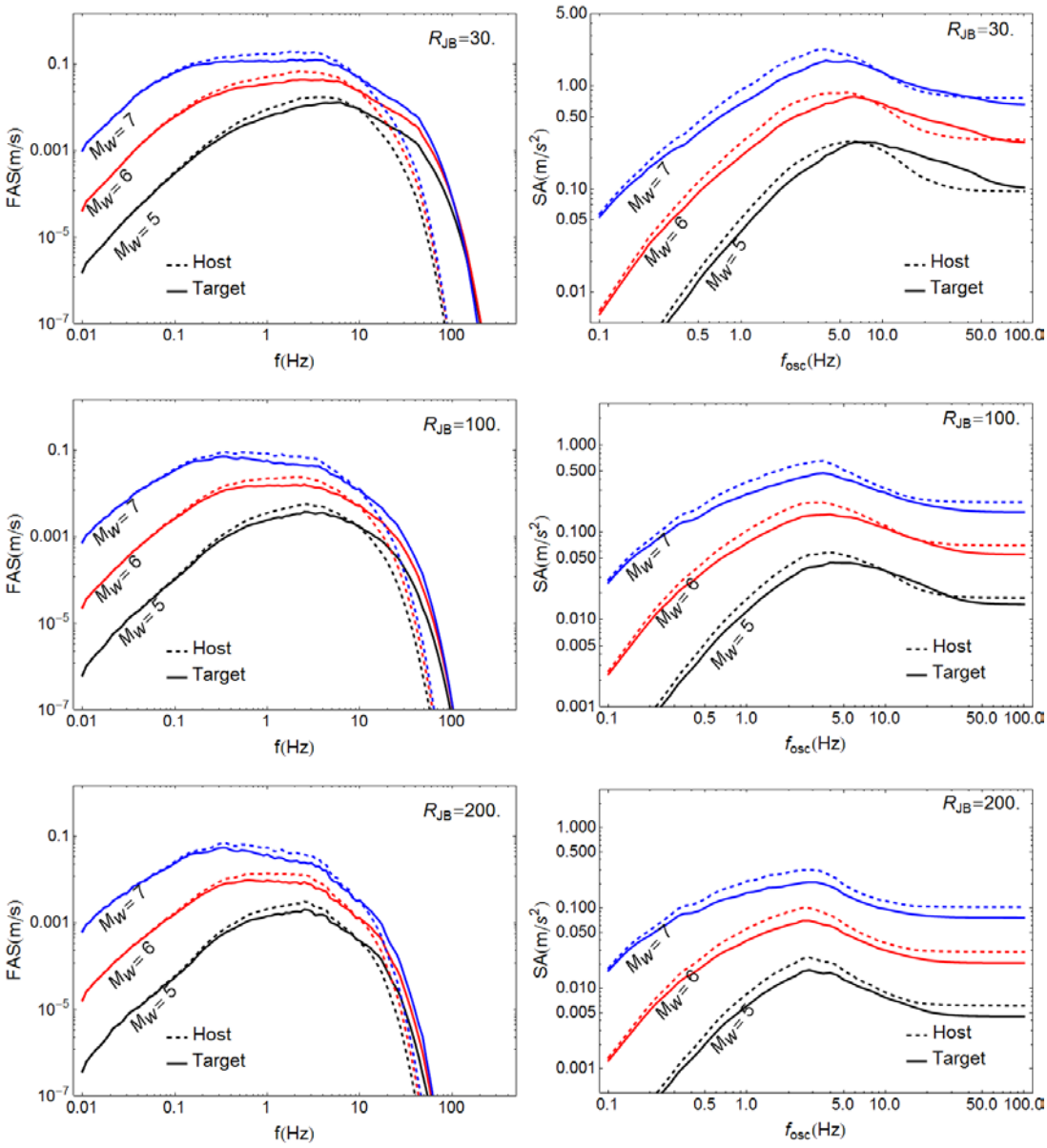

Figure 28 Plot depicting the host and target FAS (left) and corresponding response spectra (right) for the given test site 2-G. The host predictions are obtained for $\Delta\sigma$=14.5 MPa, Vs_{30}=620 m/s and κ=0.042 (s).

Subsequently the adjustments are performed following the procedure explained in the last paragraph. Figure 27 and Figure 28 depict the adjustments, for the two given sites, in the response spectral ordinates obtained by the presented approach. Left panel of Figure 27 depicts the host and target FAS corresponding to 1-V site and right panel depicts the corresponding adjustment in the response spectral ordinate corresponding to M_W 5, 6 and 7 at R_{JB}= 30, 100 and

200 km. Figure 28 depicts the identical analysis for site 2-G. It is worth emphasizing here that in the preceding computation the host parameter values for $\Delta\sigma$, Vs_{30} and κ are used as 14.5 MPa, 620 m/s and 0.042 s respectively.

9.2 Adjustment factors

As mentioned earlier, the presented approach of developing a response spectral GMPE via two empirical models for FAS and duration of ground-motion can also be used to generate the response spectral adjustment factors to be applied to the existing GMPE derived over the same database. Computation of such adjustment factors is quite straightforward with this approach; it requires the host and target response spectra obtained by the procedure as explained in the last sub-section. Subsequently, the adjustment factor at a particular oscillator-frequency is computed as the ratio of target response spectral ordinate to host response spectral ordinates at that oscillator-frequency. The computation of adjustment factors is demonstrated here for the same scenarios of magnitude and distance as shown in the previous sub-section. Figure 29 depicts the variation of adjustment factors with oscillator frequency for site 1-V corresponding to M_W 5, 6 and 7 at R_{JB} = 30, 100 and 200 km. Similarly, Figure 30 depicts the variation of adjustment factors for the test site 2-G.

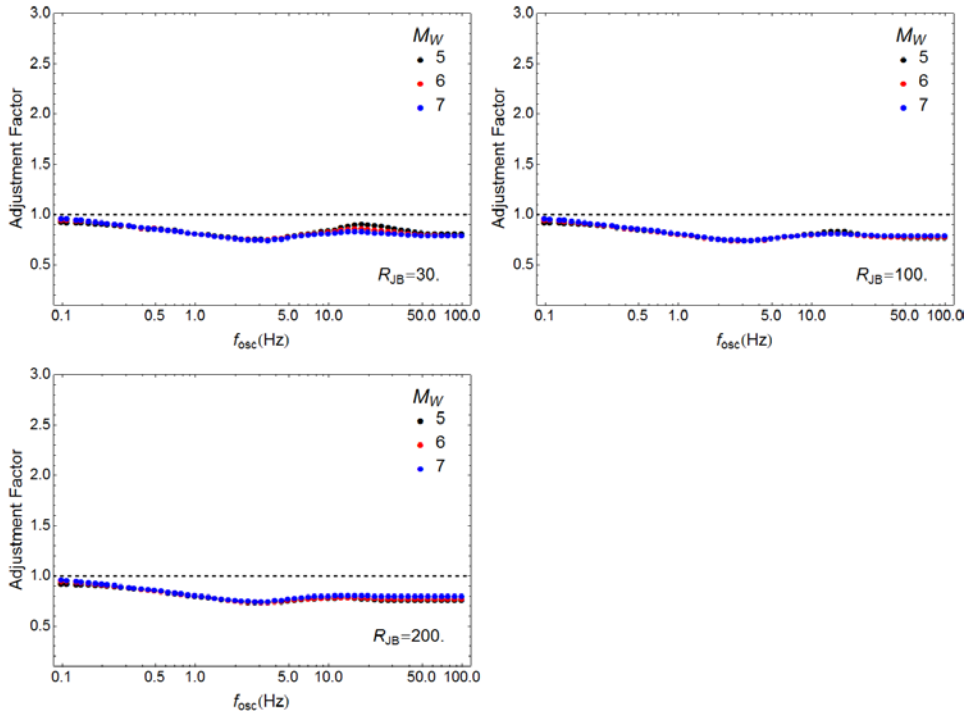

Figure 29 Plot of adjustment factors with oscillator-frequency for the given test site 1-V. The adjustment factors are computed for the same scenarios for which the adjustments have been shown in Figure 27.

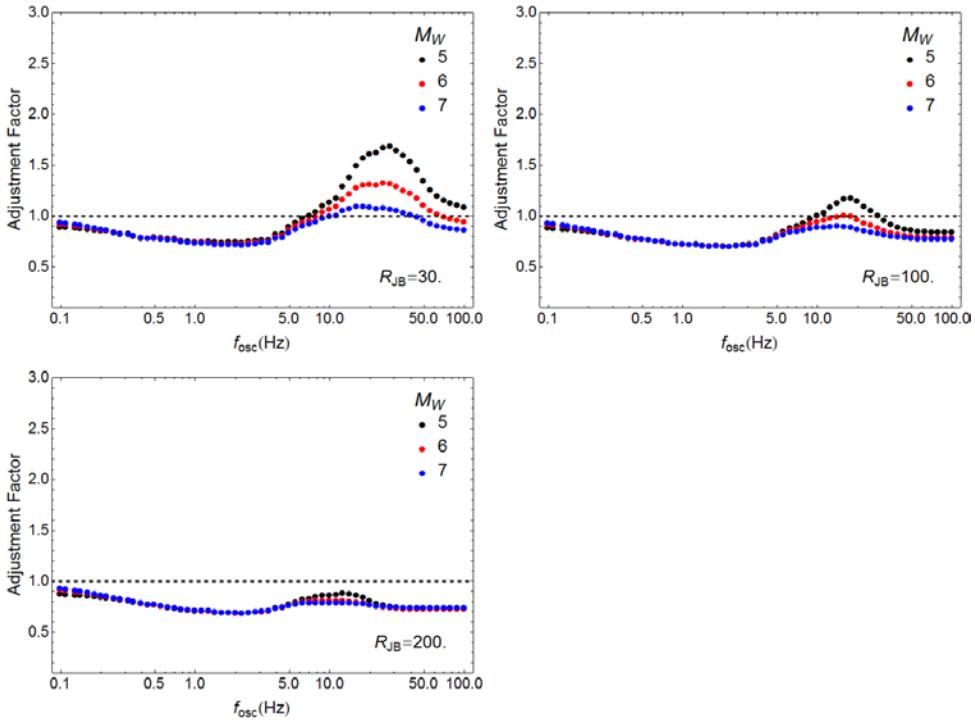

Figure 30 Plot of adjustment factors with oscillator-frequency for the given test site 2-G. The adjustment factors are computed for the same scenarios for which the adjustments have been shown in Figure 28.

10. Conclusion

This study presents a complete framework for developing a full response spectral GMPE easily adjustable to account for differences in source, path and site condition effects. Similar to the approach as described in Bora et al. (2014) it utilizes the RVT to combine the empirical models for FAS and duration. However this study presents a holistic framework for the development of response spectral GMPEs in comparison to the one presented in Bora et al. (2014). For the empirical FAS model, the data available at each frequency decides the frequency to be used for model generation. Often, the data is not sufficient beyond a band of frequencies to be used for deriving the empirical model. In order to address this issue, a stochastic model based extrapolation of Fourier amplitude spectra is proposed. Stochastic parameters that are most appropriate for the individual records are determined in the frequency range that is supported by the observed data. The determined stochastic parameters are used to extrapolate the individual spectrum by predicting the Fourier spectral amplitudes beyond the available frequency range. This enabled to derive an empirical FAS model in the frequency range 0.01-398.11 Hz. Additionally, the record-specific $\Delta\sigma$ parameter κ were included as predictor variables in the empirical model. The inclusion of $\Delta\sigma$ and κ facilitated a significant reduction in aleatory variability in comparison to the one observed in Bora et al. (2014). Moreover, an oscillator-frequency dependent duration consistent with the observed response spectra is suggested. Consequently, an empirical model was derived for duration at each oscillator frequency consisting M_W, R_{JB}, Vs_{30}, $\Delta\sigma$ and κ as the predictor variables.

Finally, the response spectrum is obtained from the predictions of both the FAS and duration models using the RVT. Comparisons of the predicted response spectra with the other RESORCE GMPEs Akkar et al. (2014), Bindi et al. (2014) are performed. In addition to that, one NGA-2 GMPE of Boore et al. (2013) is also chosen for comparison. As far as the median predicted

response spectra are concerned, predictions from present approach are found reasonably comparable with the other GMPEs considering the fact that in this study the GMPE is not derived by performing regression directly on the response spectral ordinates. One of the technical limitations of the Bora et al. (2014) was the high value of total aleatory variability associated with the median response spectral ordinates. To that end, one of the notable achievements of this study is the significant reduction in the aleatory variability of the final response spectral ordinates. The aleatory variability from this study at f_{osc}> 2.5 Hz is found to be significantly lower than that for other regional GMPEs. However, this reduction in the aleatory variability should be treated consistent with the method of developing a response spectral GMPE presented in this study. This suggests that such low values of aleatory variability can be obtained if the parameters $\Delta\sigma$ and κ are determined as suggested herein. Nevertheless, this method makes it far easier to account for the contribution of variations in these parameters (through epistemic uncertainty) in the final aleatory variability. Finally, an application of the present approach in-terms of host-to-target adjustments is demonstrated for the two given test sites. This involves adjusting the site-condition effects in terms of Vs-kappa scenarios for the two given sites.

11. Future work

- Investigating benefits/limitations of the presented approach of developing a response spectral GMPE.
- Employing the same approach over different datasets compiled in different parts of the world e.g. NGA-2 database, this is believed to provide useful insights towards deciding the functional forms of FAS and duration models.
- Investigating the variability in the final response spectral ordinates and propagation of variability of FAS and duration predictions through RVT.

- Investigation of contribution of different variability components such as source, path and site condition effects through the epistemic variability in the final response spectral variability.

12. References

Abrahamson, N. A., & Youngs, R. R. (1992). A stable algorithm for regression analyses using the random effects model. *Bulletin of the Seismological Society of America* , *82* (1), 505–510.

Abrahamson, N., Atkinson, G., Boore, D., Bozorgnia, Y., Campbell, K., Chiou, B., … Youngs, R. (2008). Comparisons of the NGA Ground-Motion Relations. *Earthquake Spectra*, *24*(1), 45–66. doi:10.1193/1.2924363

Akkar, S., Sandıkkaya, M. a., & Bommer, J. J. (2014). Empirical ground-motion models for point- and extended-source crustal earthquake scenarios in Europe and the Middle East. *Bulletin of Earthquake Engineering*, *12*(1), 359–387. doi:10.1007/s10518-013-9461-4

Anderson, J. G., & Hough, S. E. (1984). A model for the shape of the fourier amplitude spectrum of acceleration at high frequencies. *Bulletin of the Seismological Society of America* , *74* (5), 1969–1993.

Atkinson, G. M. (2004). Empirical Attenuation of Ground-Motion Spectral Amplitudes in Southeastern Canada and the Northeastern United States. *Bulletin of the Seismological Society of America* , *94* (6), 2419–2423. doi:10.1785/0120040161

Atkinson, G. M., & Boore, D. M. (2006). Earthquake Ground-Motion Prediction Equations for Eastern North America. *Bulletin of the Seismological Society of America* , *96* (6), 2181–2205. doi:10.1785/0120050245

Atkinson, G. M., & Mereu, R. F. (1992). The shape of ground motion attenuation curves in southeastern Canada. *Bulletin of the Seismological Society of America* , *82* (5), 2014–2031.

Bindi, D., Massa, M., Luzi, L., Ameri, G., Pacor, F., Puglia, R., & Augliera, P. (2014). Pan-European ground-motion prediction equations for the average horizontal component of PGA, PGV, and 5 %-damped PSA at spectral periods up to 3.0 s using the RESORCE dataset. *Bulletin of Earthquake Engineering*, *12*(1), 391–430. doi:10.1007/s10518-013-9525-5

Bommer, J. J., & Martínez-pereira, A. (1999). THE EFFECTIVE DURATION OF EARTHQUAKE STRONG MOTION. *Journal of Earthquake Engineering*, *3*(2), 127–172.

Boore, D. (1983). Stochastic Simulation of high frequency ground motions based on seismological models of the raditaed spectra. *America*, *73*(6), 1865–1894.

Boore, D. M. (2003). Simulation of Ground Motion Using the Stochastic Method. *Pure and Applied Geophysics*, *160*(3), 635–676. doi:10.1007/PL00012553

Boore, D. M. and, & Thompson, E. M. (2014). Path Durations for Use in the Stochastic-method Simulation of Ground Motions. *Bulletin of the Seismological Society of America, In press*.

Boore, D. M., & Boatwright, J. (1984). Average body-wave radiation coefficients. *Bulletin of the Seismological Society of America , 74* (5), 1615–1621.

Boore, D. M., & Bommer, J. J. (2005). Processing of strong-motion accelerograms: needs, options and consequences. *Soil Dynamics and Earthquake Engineering*, *25*(2), 93–115. doi:http://dx.doi.org/10.1016/j.soildyn.2004.10.007

Boore, D. M., & Goulet, C. a. (2014). The effect of sampling rate and anti-aliasing filters on high-frequency response spectra. *Bulletin of Earthquake Engineering*, *12*(1), 203–216. doi:10.1007/s10518-013-9574-9

Boore, D. M., & Joyner, W. B. (1997). Site amplifications for generic rock sites. *Bulletin of the Seismological Society of America , 87* (2), 327–341.

Boore, D. M., Stewart, J. P., Seyhan, E., & Atkinson, G. M. (2013). NGA-West2 Equations for Predicting PGA, PGV, and 5% Damped PSA for Shallow Crustal Earthquakes. *Earthquake Spectra*, *30*(3), 1057–1085. doi:10.1193/070113EQS184M

Boore, D. M., & Thompson, E. M. (2012). Empirical Improvements for Estimating Earthquake Response Spectra with Random-Vibration Theory. *Bulletin of the Seismological Society of America , 102* (2), 761–772. doi:10.1785/0120110244

Bora, S. S., Scherbaum, F., Kuehn, N., & Stafford, P. (2014). Fourier spectral- and duration models for the generation of response spectra adjustable to different source-, propagation-, and site conditions. *Bulletin of Earthquake Engineering*, *12*(1), 467–493. doi:10.1007/s10518-013-9482-z

Brune, J. (1970). Tectonic Stress and the Spectra of Seismic Shear Waves from Earthquakes. *Journal of Geophysical Reasearch*, *75*(26), 4997–5009.

Brune, J. (1971). Correction. *Journal of Geophysical Reasearch*, *76*(20), 5002.

Campillo, M., Bouchon, M., & Massinon, B. (1984). Theoretical study of the excitation, spectral characteristics, and geometrical attenuation of regional seismic phases. *Bulletin of the Seismological Society of America , 74* (1), 79–90.

Cartwright, DE and Longuet-Higgins, M. S. (1956). The statistical distribution of the maxima of a Random function. *Proceedings of the Royal Soceity of London. Series A, Mathematical and Physical Sciences*, *237*(1209), 212–232.

Cotton, F., Scherbaum, F., Bommer, J., & Bungum, H. (2006). Criteria for Selecting and Adjusting Ground-Motion Models for Specific Target Regions: Application to Central Europe and Rock Sites. *Journal of Seismology*, *10*(2), 137–156. doi:10.1007/s10950-005-9006-7

Douglas, J., Akkar, S., Ameri, G., Bard, P.-Y., Bindi, D., Bommer, J. J., … Traversa, P. (2013). Comparisons among the five ground-motion models developed using RESORCE for the prediction of response spectral accelerations due to earthquakes in Europe and the Middle East. *Bulletin of Earthquake Engineering*, *12*(1), 341–358. doi:10.1007/s10518-013-9522-8

Drouet, S., Cotton, F., & Guéguen, P. (2010). VS30, κ, regional attenuation and Mw from accelerograms: Application to magnitude 3-5 French earthquakes. *Geophysical Journal International*, *182*(2), 880–898.

Edwards, B., & Fah, D. (2013). Measurements of stress parameter and site attenuation from recordings of moderate to large earthquakes in Europe and the Middle East. *Geophysical Journal International*, *194*(2), 1190–1202. doi:10.1093/gji/ggt158

Edwards, B., Michel, C., Poggi, V., & Fäh, D. (2013). Determination of Site Amplification from Regional Seismicity: Application to the Swiss National Seismic Networks. *Seismological Research Letters* , *84* (4), 611–621. doi:10.1785/0220120176

Edwards, B., Rietbrock, A., Bommer, J. J., & Baptie, B. (2008). The Acquisition of Source, Path, and Site Effects from Microearthquake Recordings Using Q Tomography: Application to the United Kingdom. *Bulletin of the Seismological Society of America* , *98* (4), 1915–1935. doi:10.1785/0120070127

Eshelby, J. D. (1957). No Title. In *The determination of the elastic field of an ellipsoidal inclusion, and related problems* (pp. 376–396). Proc R Soc Lon Ser.

Hanks, T. C., & Kanamori, H. (1979). A moment magnitude scale. In *Journal of Geophysical Research B: Solid Earth* (Vol. 84, pp. 2348–2350).

Hanks, T. C., & McGuire, R. K. (1981). The character of high-frequency strong ground motion. *Bulletin of the Seismological Society of America* , *71* (6), 2071–2095.

Madariaga, R. (1976). Dynamics of an expanding circular fault. *Bulletin of the Seismological Society of America* , *66* (3), 639–666.

Poggi, V., Edwards, B., & Fäh, D. (2011). Derivation of a Reference Shear-Wave Velocity Model from Empirical Site Amplification. *Bulletin of the Seismological Society of America* , *101* (1), 258–274. doi:10.1785/0120100060

Rietbrock, A., Strasser, F., & Edwards, B. (2013). A Stochastic Earthquake Ground-Motion Prediction Model for the United Kingdom. *Bulletin of the Seismological Society of America* , *103* (1), 57–77. doi:10.1785/0120110231

Scherbaum, F. (1990). Combined inversion for the three-dimensional Q structure and source parameters using microearthquake spectra. *Journal of Geophysical Research: Solid Earth, 95*(B8), 12423–12438. doi:10.1029/JB095iB08p12423

Thatcher, W., & Hanks, T. C. (1973). Source parameters of southern California earthquakes. *Journal of Geophysical Research, 78*(35), 8547–8576. doi:10.1029/JB078i035p08547

Vanmarcke, E. H., & Lai, S.-S. P. (1980). Strong-motion duration and RMS amplitude of earthquake records. *Bulletin of the Seismological Society of America , 70* (4), 1293–1307.

13. Appendix

Table 1 Coefficients involved in equation (7).

f(hz)	c_0	c_1	c_2	c_3	c_4	c_5	c_6	c_7	φ	τ	σ
0.01	-20.157	3.054	-0.058	-2.034	0.257	3.106	0	-0.694	0.784	0.388	0.875
0.011	-20.636	3.358	-0.083	-1.959	0.244	3.152	0	-0.691	0.761	0.381	0.852
0.012	-20.993	3.537	-0.092	-1.813	0.22	3.08	0	-0.72	0.78	0.4	0.876
0.013	-20.892	3.501	-0.091	-1.809	0.223	3.039	0	-0.696	0.778	0.411	0.88
0.014	-20.085	3.322	-0.078	-1.845	0.228	3.171	0	-0.697	0.789	0.423	0.895
0.016	-20.359	3.568	-0.098	-1.818	0.221	3.105	0	-0.718	0.778	0.406	0.877
0.017	-20.014	3.48	-0.09	-1.797	0.22	2.978	0	-0.723	0.781	0.413	0.884
0.019	-20.671	3.736	-0.108	-1.654	0.192	3.537	0	-0.707	0.771	0.428	0.882
0.021	-20.143	3.449	-0.074	-1.432	0.158	3.506	0	-0.684	0.773	0.439	0.889
0.023	-20.283	3.626	-0.093	-1.507	0.167	3.551	0	-0.677	0.765	0.438	0.881
0.025	-20.129	3.789	-0.114	-1.623	0.183	3.518	0	-0.697	0.745	0.452	0.872
0.028	-21.407	4.238	-0.152	-1.624	0.178	4.85	0	-0.646	0.724	0.433	0.844
0.03	-22.643	4.535	-0.162	-1.32	0.123	4.892	0	-0.634	0.718	0.481	0.864
0.033	-22.675	4.535	-0.163	-1.351	0.129	4.54	0	-0.599	0.725	0.495	0.877
0.036	-22.194	4.548	-0.168	-1.488	0.145	5.932	0	-0.595	0.697	0.507	0.862
0.04	-22.71	4.825	-0.191	-1.519	0.144	6.241	0	-0.592	0.691	0.493	0.849
0.044	-23.813	5.313	-0.236	-1.568	0.149	6.516	0	-0.583	0.702	0.505	0.865
0.048	-24.092	5.421	-0.244	-1.516	0.138	6.316	0	-0.566	0.705	0.486	0.856
0.052	-24.526	5.595	-0.259	-1.47	0.132	6.213	0	-0.558	0.709	0.501	0.868
0.058	-24.091	5.577	-0.263	-1.59	0.147	7.281	0	-0.534	0.682	0.524	0.86
0.063	-24.304	5.843	-0.295	-1.714	0.165	7.163	0	-0.536	0.689	0.508	0.856
0.069	-24.864	6.062	-0.319	-1.743	0.171	7.336	0	-0.493	0.693	0.492	0.85
0.076	-25.198	6.233	-0.331	-1.652	0.155	7.209	0	-0.507	0.695	0.545	0.883
0.083	-25.15	6.4	-0.355	-1.775	0.175	7.646	0	-0.515	0.695	0.544	0.882
0.091	-23.335	5.965	-0.325	-1.858	0.187	8.203	0	-0.532	0.691	0.548	0.882
0.1	-22.756	5.942	-0.33	-1.947	0.203	7.693	0	-0.552	0.69	0.554	0.885

f(hz)	c_0	c_1	c_2	c_3	c_4	c_5	c_6	c_7	φ	τ	σ
0.11	-22.409	5.957	-0.335	-1.932	0.202	6.937	0	-0.575	0.693	0.555	0.888
0.12	-20.991	5.62	-0.315	-2.027	0.221	6.765	0	-0.591	0.692	0.58	0.902
0.132	-21.574	5.88	-0.337	-1.953	0.209	7.242	0	-0.591	0.685	0.579	0.897
0.145	-20.318	5.639	-0.328	-2.07	0.231	6.379	0	-0.603	0.689	0.568	0.893
0.158	-21.004	5.936	-0.352	-1.984	0.217	6.441	0	-0.616	0.69	0.566	0.893
0.174	-21.183	6.055	-0.362	-1.851	0.198	5.764	0	-0.635	0.695	0.594	0.915
0.191	-21.519	6.27	-0.381	-1.741	0.182	5.11	0	-0.664	0.696	0.608	0.924
0.209	-21.11	6.182	-0.375	-1.645	0.167	4.563	0	-0.671	0.705	0.606	0.93
0.229	-20.808	6.254	-0.386	-1.635	0.167	4.379	0	-0.713	0.72	0.618	0.949
0.251	-20.022	6.112	-0.377	-1.602	0.164	3.746	0	-0.748	0.737	0.628	0.968
0.275	-18.837	5.861	-0.362	-1.632	0.172	3.138	0	-0.78	0.766	0.631	0.992
0.302	-17.95	5.711	-0.354	-1.618	0.172	3.068	0	-0.82	0.786	0.642	1.015
0.331	-17.544	5.688	-0.358	-1.649	0.177	2.96	0	-0.824	0.797	0.618	1.009
0.363	-17.254	5.673	-0.36	-1.636	0.172	3.226	0	-0.82	0.802	0.581	0.99
0.398	-17.458	5.914	-0.384	-1.602	0.16	3.917	0	-0.849	0.797	0.546	0.966
0.437	-16.938	5.898	-0.384	-1.566	0.15	3.726	0	-0.892	0.796	0.513	0.947
0.479	-16.514	5.824	-0.378	-1.505	0.138	3.76	0	-0.901	0.81	0.492	0.948
0.525	-14.433	5.215	-0.332	-1.55	0.147	3.512	0	-0.915	0.803	0.479	0.935
0.575	-13.972	5.158	-0.333	-1.553	0.149	3.409	0	-0.925	0.785	0.469	0.914
0.631	-13.55	5.081	-0.324	-1.44	0.129	3.121	0	-0.962	0.784	0.448	0.903
0.692	-12.499	4.881	-0.304	-1.347	0.111	3.313	0	-1.037	0.788	0.439	0.902
0.759	-11.952	4.802	-0.298	-1.326	0.102	3.543	0	-1.057	0.769	0.431	0.881
0.832	-11.532	4.68	-0.292	-1.376	0.103	4.434	0	-1.012	0.758	0.421	0.867
0.912	-11.115	4.567	-0.283	-1.338	0.093	3.849	0	-1.004	0.744	0.417	0.853
1	-10.189	4.353	-0.272	-1.435	0.109	4.288	0	-1.004	0.734	0.413	0.842
1.096	-10.476	4.567	-0.293	-1.425	0.102	5.046	0	-1.019	0.734	0.411	0.841
1.202	-10.155	4.396	-0.272	-1.294	0.072	5.28	0	-0.993	0.72	0.428	0.837
1.318	-9.508	4.219	-0.265	-1.383	0.088	4.901	0	-0.974	0.725	0.432	0.844
1.445	-8.233	3.823	-0.233	-1.46	0.094	5.891	0	-0.953	0.726	0.417	0.837
1.585	-10.032	4.178	-0.257	-1.302	0.06	6.378	0	-0.836	0.728	0.414	0.837
1.738	-10.051	4.131	-0.248	-1.284	0.044	6.931	0	-0.788	0.735	0.417	0.845
1.905	-9.947	4.059	-0.244	-1.298	0.044	6.79	0	-0.744	0.718	0.427	0.835
2.089	-8.767	3.762	-0.232	-1.456	0.069	7.865	0	-0.715	0.713	0.386	0.811
2.291	-8.546	3.548	-0.209	-1.424	0.051	8.738	0	-0.626	0.71	0.36	0.796
2.512	-9.619	3.753	-0.231	-1.375	0.05	7.589	0	-0.559	0.727	0.376	0.819
2.754	-8.384	3.148	-0.174	-1.326	0.031	8.361	0	-0.472	0.707	0.357	0.792
3.02	-6.852	2.836	-0.157	-1.538	0.062	8.463	0	-0.502	0.711	0.368	0.8
3.311	-6.366	2.542	-0.137	-1.571	0.078	8.639	0.002	-0.433	0.678	0.387	0.781
3.631	-5.891	2.301	-0.119	-1.596	0.077	9.295	0.002	-0.369	0.708	0.367	0.797
3.981	-6.336	2.513	-0.123	-1.446	0.02	12.287	0.001	-0.376	0.742	0.342	0.817
4.365	-4.692	2.062	-0.101	-1.757	0.061	12.93	0.001	-0.311	0.719	0.359	0.804

f(hz)	c_0	c_1	c_2	c_3	c_4	c_5	c_6	c_7	φ	τ	σ
4.786	-5.983	2.414	-0.133	-1.682	0.059	12.712	0.003	-0.281	0.69	0.346	0.772
5.248	-6.455	2.395	-0.131	-1.579	0.05	12.842	0.004	-0.234	0.709	0.372	0.8
5.754	-5.997	2.38	-0.127	-1.838	0.044	16.207	0.002	-0.151	0.722	0.384	0.818
6.31	-6.357	2.328	-0.129	-1.776	0.052	15.795	0.004	-0.103	0.74	0.416	0.849
6.918	-6.972	2.466	-0.135	-1.819	0.028	16.541	0.003	-0.027	0.75	0.403	0.852
7.586	-7.015	2.134	-0.109	-1.784	0.037	15.722	0.004	0.087	0.756	0.413	0.862
8.318	-8.087	2.127	-0.104	-1.5	0.007	13.924	0.005	0.15	0.789	0.419	0.894
9.12	-7.633	1.839	-0.09	-1.548	0.031	13.183	0.007	0.2	0.795	0.437	0.907
10	-8.292	1.973	-0.105	-1.713	0.053	13.611	0.007	0.272	0.802	0.47	0.93
10.965	-8.61	2.061	-0.113	-1.677	0.042	14.096	0.006	0.262	0.85	0.413	0.946
12.023	-8.434	1.967	-0.086	-1.589	-0.013	15.454	0.005	0.283	0.883	0.422	0.979
13.183	-9.13	1.831	-0.078	-1.388	-0.011	13.751	0.006	0.317	0.927	0.441	1.026
14.454	-8.814	1.601	-0.054	-1.383	-0.023	13.604	0.007	0.357	0.976	0.453	1.076
15.849	-9.959	1.859	-0.067	-1.17	-0.057	13.048	0.007	0.327	1.074	0.465	1.17
17.378	-12.007	2.09	-0.085	-1.021	-0.064	11.606	0.009	0.445	1.135	0.468	1.227
19.055	-12.823	1.969	-0.062	-0.697	-0.107	11.377	0.012	0.493	1.206	0.496	1.304
20.893	-14.613	2.144	-0.068	-0.533	-0.133	11.083	0.013	0.618	1.297	0.514	1.395
22.909	-14.235	1.866	-0.035	-0.487	-0.153	11.462	0.014	0.64	1.409	0.571	1.52
25.119	-15.429	1.838	-0.021	-0.387	-0.189	11.067	0.014	0.783	1.584	0.614	1.699
27.542	-16.657	2.054	-0.014	-0.228	-0.27	13.928	0.013	0.875	1.751	0.662	1.872
30.2	-19.18	2.349	-0.008	0.124	-0.354	14.649	0.015	1.001	1.911	0.739	2.049
33.113	-20.353	2.367	0.009	0.264	-0.409	15.013	0.016	1.131	2.106	0.812	2.258
36.308	-20.965	2.031	0.05	0.416	-0.443	14.344	0.017	1.28	2.324	0.897	2.491
39.811	-23.101	2.319	0.065	0.667	-0.553	16.168	0.017	1.438	2.564	1.018	2.758
43.652	-25.362	2.467	0.089	0.971	-0.653	16.744	0.018	1.611	2.845	1.136	3.063
47.863	-25.221	1.892	0.147	0.91	-0.67	17.58	0.018	1.803	3.146	1.241	3.382
52.481	-31.251	2.66	0.16	1.97	-0.902	19.482	0.02	2.067	3.42	1.343	3.674
57.544	-34.649	2.937	0.182	2.447	-1.037	20.349	0.022	2.31	3.768	1.473	4.046
63.096	-38.448	3.258	0.206	2.986	-1.189	21.242	0.023	2.576	4.152	1.616	4.455
69.183	-42.716	3.64	0.232	3.588	-1.359	22.148	0.025	2.867	4.574	1.774	4.906
75.858	-47.471	4.074	0.26	4.269	-1.552	23.081	0.027	3.187	5.038	1.948	5.402
83.176	-52.772	4.575	0.292	5.031	-1.767	24.01	0.029	3.538	5.548	2.14	5.946
91.201	-58.642	5.138	0.326	5.878	-2.006	24.91	0.031	3.923	6.108	2.35	6.545
100	-65.216	5.795	0.364	6.831	-2.276	25.842	0.033	4.345	6.723	2.581	7.202
109.648	-72.478	6.529	0.405	7.888	-2.575	26.734	0.035	4.808	7.398	2.836	7.923
120.226	-80.531	7.356	0.45	9.063	-2.907	27.594	0.038	5.316	8.14	3.115	8.715
131.826	-89.438	8.283	0.499	10.366	-3.275	28.426	0.04	5.873	8.953	3.421	9.584
144.544	-99.289	9.323	0.552	11.81	-3.682	29.226	0.043	6.484	9.845	3.757	10.538
158.489	-110.142	10.474	0.611	13.405	-4.131	29.979	0.046	7.154	10.824	4.127	11.584
173.78	-121.33	11.414	0.674	15.022	-4.548	30	0.052	7.888	11.897	4.531	12.731
190.546	-133.553	12.428	0.743	16.79	-5.002	30	0.058	8.691	13.075	4.975	13.99

f(hz)	c_0	c_1	c_2	c_3	c_4	c_5	c_6	c_7	φ	τ	σ
208.93	-146.949	13.543	0.818	18.723	-5.5	30	0.065	9.572	14.367	5.462	15.371
229.087	-161.695	14.773	0.9	20.855	-6.047	30	0.072	10.539	15.784	5.997	16.885
251.189	-177.645	16.079	0.993	23.157	-6.643	30	0.081	11.597	17.338	6.583	18.546
275.423	-195.286	17.536	1.093	25.706	-7.298	30	0.089	12.76	19.043	7.225	20.367
301.995	-215.205	19.266	1.196	28.596	-8.033	30	0.099	14.037	20.911	7.931	22.365
331.131	-235.77	20.893	1.321	31.545	-8.803	30	0.11	15.429	22.961	8.703	24.555
363.078	-258.768	22.756	1.456	34.869	-9.662	30	0.122	16.959	25.208	9.551	26.957
398.107	-284.817	24.985	1.595	38.647	-10.625	30	0.135	18.641	27.673	10.481	29.591

Table 2 Coefficients involved in equation (8).

f(hz)	c_0	c_1	c_2	c_3	c_4	c_5	c_6	c_7	c_8	ϕ	τ	σ
0.01	-20.002	3.011	-0.055	-2.048	0.259	3.271	0	-0.695	0	0.784	0.388	0.875
0.011	-20.678	3.376	-0.085	-1.962	0.244	3.15	0	-0.691	0	0.761	0.381	0.852
0.012	-20.871	3.501	-0.09	-1.823	0.221	3.267	0	-0.721	0	0.78	0.4	0.876
0.013	-20.896	3.503	-0.091	-1.81	0.222	3.109	0	-0.696	0	0.778	0.411	0.88
0.014	-20.043	3.315	-0.078	-1.854	0.23	3.181	0	-0.697	0	0.789	0.423	0.895
0.016	-20.349	3.565	-0.098	-1.82	0.222	3.088	0	-0.718	0	0.778	0.407	0.877
0.017	-20.032	3.49	-0.091	-1.801	0.221	2.982	0	-0.723	0	0.781	0.413	0.884
0.019	-20.648	3.733	-0.108	-1.659	0.193	3.554	0	-0.708	0	0.771	0.428	0.882
0.021	-20.18	3.467	-0.076	-1.436	0.159	3.529	0	-0.684	0	0.773	0.439	0.889
0.023	-20.333	3.644	-0.095	-1.506	0.167	3.591	0	-0.677	0	0.765	0.438	0.881
0.025	-20.134	3.794	-0.115	-1.624	0.183	3.531	0	-0.697	0	0.745	0.452	0.872
0.028	-21.401	4.238	-0.152	-1.625	0.179	4.87	0	-0.646	0	0.724	0.433	0.844
0.03	-22.628	4.529	-0.161	-1.321	0.123	4.841	0	-0.634	0	0.718	0.481	0.864
0.033	-22.645	4.526	-0.162	-1.353	0.13	4.548	0	-0.599	0	0.725	0.495	0.877
0.036	-22.194	4.549	-0.168	-1.488	0.144	5.929	0	-0.595	0	0.697	0.507	0.862
0.04	-22.752	4.841	-0.193	-1.518	0.144	6.24	0	-0.592	0	0.691	0.493	0.849
0.044	-23.831	5.321	-0.236	-1.568	0.149	6.553	0	-0.584	0	0.702	0.505	0.865
0.048	-24.074	5.418	-0.244	-1.519	0.139	6.337	0	-0.566	0	0.705	0.486	0.856
0.052	-24.5	5.587	-0.258	-1.472	0.132	6.193	0	-0.558	0	0.709	0.501	0.868
0.058	-24.125	5.587	-0.264	-1.587	0.147	7.264	0	-0.534	0	0.682	0.524	0.86
0.063	-24.339	5.853	-0.296	-1.711	0.164	7.157	0	-0.535	0	0.689	0.508	0.856
0.069	-24.853	6.062	-0.319	-1.745	0.171	7.386	0	-0.493	0	0.693	0.492	0.849
0.076	-25.158	6.224	-0.331	-1.658	0.157	7.124	0	-0.508	0	0.695	0.545	0.883
0.083	-25.173	6.406	-0.356	-1.774	0.175	7.617	0	-0.515	0	0.695	0.544	0.882
0.091	-23.334	5.967	-0.325	-1.86	0.187	8.212	0	-0.532	0	0.691	0.548	0.882
0.1	-22.751	5.943	-0.33	-1.949	0.203	7.72	0	-0.552	0	0.69	0.554	0.885
0.11	-22.409	5.954	-0.335	-1.929	0.202	6.925	0	-0.574	0	0.693	0.555	0.888
0.12	-21.012	5.624	-0.315	-2.024	0.221	6.792	0	-0.59	0	0.692	0.58	0.902

0.132	-21.53	5.867	-0.336	-1.955	0.209	7.33	0	-0.591	0	0.685	0.579	0.897
0.145	-20.294	5.636	-0.328	-2.075	0.232	6.52	0	-0.603	0	0.689	0.568	0.893
0.158	-20.981	5.937	-0.353	-1.994	0.219	6.443	0	-0.616	0	0.69	0.566	0.893
0.174	-21.201	6.066	-0.363	-1.855	0.199	5.771	0	-0.635	0	0.695	0.594	0.915
0.191	-21.576	6.292	-0.383	-1.743	0.182	5.129	0	-0.664	0	0.696	0.608	0.924
0.209	-21.099	6.191	-0.376	-1.654	0.168	4.713	0	-0.672	0	0.705	0.606	0.93
0.229	-20.832	6.277	-0.389	-1.646	0.169	4.546	0	-0.714	0	0.72	0.618	0.949
0.251	-20.061	6.138	-0.38	-1.609	0.165	3.929	0	-0.749	0	0.737	0.627	0.968
0.275	-18.875	5.884	-0.364	-1.637	0.172	3.326	0	-0.781	0	0.766	0.631	0.992
0.302	-18.017	5.749	-0.358	-1.627	0.173	3.245	0	-0.821	0	0.787	0.641	1.015
0.331	-17.846	5.807	-0.369	-1.65	0.177	3.17	0	-0.825	0	0.797	0.618	1.008
0.363	-17.297	5.689	-0.362	-1.637	0.173	3.188	0	-0.82	0	0.802	0.581	0.99
0.398	-17.476	5.922	-0.385	-1.6	0.16	4.043	0	-0.848	0	0.797	0.546	0.966
0.437	-16.978	5.914	-0.386	-1.567	0.151	3.724	0	-0.892	0	0.796	0.513	0.947
0.479	-16.566	5.846	-0.38	-1.505	0.138	3.787	0	-0.901	0	0.81	0.492	0.948
0.525	-14.474	5.231	-0.334	-1.551	0.147	3.481	0	-0.915	0	0.803	0.479	0.935
0.575	-14.026	5.182	-0.336	-1.557	0.149	3.413	0	-0.925	0	0.785	0.469	0.914
0.631	-13.579	5.093	-0.325	-1.44	0.129	3.126	0	-0.963	0	0.784	0.448	0.903
0.692	-12.535	4.897	-0.306	-1.349	0.111	3.316	0	-1.037	0	0.788	0.439	0.902
0.759	-11.974	4.811	-0.299	-1.327	0.102	3.539	0	-1.057	0	0.769	0.431	0.881
0.832	-11.581	4.698	-0.294	-1.378	0.104	4.37	0	-1.012	0	0.758	0.421	0.867
0.912	-11.149	4.581	-0.285	-1.338	0.093	3.851	0	-1.004	0	0.744	0.417	0.853
1	-10.214	4.367	-0.274	-1.438	0.109	4.348	0	-1.004	0	0.734	0.413	0.842
1.096	-10.498	4.576	-0.294	-1.423	0.101	5.13	0	-1.019	0	0.734	0.411	0.841
1.202	-10.192	4.412	-0.274	-1.296	0.072	5.282	0	-0.993	0	0.72	0.428	0.837
1.318	-9.531	4.229	-0.266	-1.385	0.088	4.906	0	-0.974	0	0.725	0.432	0.844
1.445	-8.26	3.835	-0.234	-1.461	0.094	5.935	0	-0.953	0	0.726	0.416	0.837
1.585	-10.066	4.19	-0.258	-1.303	0.061	6.317	0	-0.835	0	0.728	0.414	0.837
1.738	-10.09	4.147	-0.249	-1.284	0.044	6.937	0	-0.788	0	0.735	0.417	0.845
1.905	-9.998	4.078	-0.246	-1.299	0.044	6.743	0	-0.744	0	0.718	0.427	0.835
2.089	-8.78	3.768	-0.232	-1.458	0.07	7.865	0	-0.715	0	0.713	0.386	0.811
2.291	-8.561	3.553	-0.209	-1.424	0.051	8.739	0	-0.626	0	0.71	0.36	0.796
2.512	-9.647	3.764	-0.232	-1.376	0.05	7.597	0	-0.559	0	0.727	0.376	0.818
2.754	-8.422	3.163	-0.175	-1.326	0.031	8.363	0	-0.472	0	0.707	0.357	0.792
3.02	-6.897	2.853	-0.159	-1.537	0.062	8.466	0	-0.502	0	0.711	0.367	0.8
3.311	-6.403	2.555	-0.138	-1.571	0.077	8.641	0.002	-0.433	0	0.678	0.387	0.781
3.631	-5.93	2.314	-0.12	-1.594	0.076	9.303	0.002	-0.369	0	0.708	0.366	0.797
3.981	-6.301	2.53	-0.125	-1.455	0.022	12.291	0.001	-0.383	0.477	0.743	0.34	0.817
4.365	-4.535	2.084	-0.105	-1.783	0.067	12.951	0.001	-0.331	1.256	0.719	0.356	0.802
4.786	-5.697	2.445	-0.139	-1.727	0.068	12.753	0.003	-0.313	2.112	0.69	0.341	0.77
5.248	-5.896	2.444	-0.142	-1.666	0.069	12.872	0.005	-0.294	3.968	0.705	0.36	0.792
5.754	-5.171	2.424	-0.141	-1.973	0.072	16.373	0.002	-0.23	5.074	0.715	0.371	0.806

6.31	-5.259	2.391	-0.148	-1.956	0.089	16.012	0.005	-0.208	6.789	0.729	0.393	0.828
6.918	-5.596	2.515	-0.155	-2.044	0.074	16.807	0.003	-0.15	7.901	0.732	0.385	0.827
7.586	-5.648	2.215	-0.133	-2.005	0.082	16.029	0.004	-0.045	8.437	0.739	0.381	0.832
8.318	-6.405	2.219	-0.132	-1.758	0.062	14.103	0.006	-0.017	10.695	0.758	0.386	0.851
9.12	-5.579	1.948	-0.123	-1.858	0.097	13.391	0.008	-0.004	13.035	0.748	0.391	0.844
10	-5.899	2.066	-0.141	-2.081	0.13	13.867	0.008	0.048	14.333	0.741	0.43	0.857
10.965	-6.027	2.168	-0.153	-2.061	0.129	14.016	0.008	0.008	16.442	0.773	0.364	0.854
12.023	-5.224	2.053	-0.132	-2.077	0.095	15.521	0.006	-0.012	19.207	0.776	0.369	0.859
13.183	-5.219	1.936	-0.132	-1.965	0.116	13.796	0.008	-0.046	23.783	0.761	0.376	0.849
14.454	-4.269	1.683	-0.114	-2.051	0.127	13.407	0.009	-0.057	27.242	0.76	0.391	0.855
15.849	-4.781	1.983	-0.137	-1.916	0.112	12.837	0.01	-0.158	31.993	0.794	0.389	0.884
17.378	-6.355	2.237	-0.162	-1.808	0.121	10.705	0.012	-0.1	36.378	0.772	0.409	0.874
19.055	-6.693	2.182	-0.152	-1.541	0.1	9.628	0.015	-0.125	41.043	0.768	0.387	0.86
20.893	-7.805	2.375	-0.166	-1.44	0.091	9.232	0.018	-0.073	45.978	0.77	0.387	0.862
22.909	-6.506	2.134	-0.15	-1.533	0.108	8.978	0.019	-0.147	52.227	0.771	0.388	0.863
25.119	-6.879	2.234	-0.156	-1.52	0.099	8.595	0.02	-0.123	60.216	0.82	0.345	0.89
27.542	-6.002	2.322	-0.166	-1.721	0.098	11.866	0.02	-0.162	68.837	0.808	0.362	0.885
30.2	-6.951	2.576	-0.178	-1.611	0.077	11.887	0.023	-0.165	77.363	0.783	0.378	0.87
33.113	-6.678	2.62	-0.184	-1.671	0.079	11.818	0.025	-0.179	86.997	0.777	0.364	0.858
36.308	-6.099	2.414	-0.17	-1.66	0.088	10.56	0.028	-0.19	97.49	0.772	0.35	0.848
39.811	-5.573	2.58	-0.181	-1.856	0.082	12.683	0.029	-0.214	109.194	0.76	0.353	0.838
43.652	-5.373	2.658	-0.185	-1.918	0.078	12.841	0.031	-0.242	122.347	0.755	0.371	0.841
47.863	-2.845	2.042	-0.16	-2.345	0.163	12.888	0.034	-0.262	135.989	0.771	0.374	0.857
52.481	-6.262	2.623	-0.183	-1.744	0.073	12.934	0.039	-0.181	148.512	0.776	0.369	0.859
57.544	-6.625	2.781	-0.199	-1.743	0.07	13.053	0.043	-0.179	164.349	0.781	0.371	0.865
63.096	-7.028	2.955	-0.216	-1.741	0.068	13.169	0.048	-0.177	181.719	0.787	0.374	0.871
69.183	-7.486	3.15	-0.235	-1.741	0.065	13.304	0.053	-0.175	200.777	0.794	0.377	0.879
75.858	-7.962	3.353	-0.255	-1.741	0.061	13.44	0.058	-0.173	221.676	0.802	0.381	0.888
83.176	-8.549	3.591	-0.278	-1.735	0.057	13.54	0.064	-0.17	244.577	0.812	0.385	0.899
91.201	-9.121	3.844	-0.303	-1.74	0.054	13.718	0.07	-0.168	269.703	0.824	0.39	0.912
100	-9.785	4.124	-0.33	-1.74	0.049	13.861	0.077	-0.165	297.244	0.838	0.397	0.927
109.648	-10.503	4.431	-0.36	-1.741	0.045	14.008	0.085	-0.162	327.445	0.855	0.404	0.945
120.226	-11.304	4.772	-0.394	-1.742	0.039	14.159	0.093	-0.159	360.568	0.874	0.412	0.967
131.826	-12.169	5.143	-0.43	-1.744	0.034	14.311	0.102	-0.155	396.872	0.897	0.422	0.992
144.544	-13.136	5.557	-0.471	-1.747	0.027	14.465	0.112	-0.151	436.692	0.924	0.433	1.021
158.489	-14.164	5.999	-0.514	-1.75	0.02	14.621	0.123	-0.146	480.351	0.955	0.447	1.055
173.78	-15.305	6.49	-0.562	-1.755	0.013	14.774	0.135	-0.141	528.217	0.992	0.463	1.094
190.546	-16.559	7.029	-0.615	-1.759	0.005	14.924	0.148	-0.135	580.704	1.034	0.481	1.14
208.93	-17.928	7.62	-0.673	-1.766	-0.004	15.07	0.163	-0.129	638.26	1.082	0.502	1.193
229.087	-19.436	8.271	-0.737	-1.774	-0.014	15.21	0.179	-0.123	701.363	1.137	0.526	1.253
251.189	-28.095	9.155	-0.841	-0.177	0.021	0.001	0.214	-0.077	770.531	1.202	0.592	1.34
275.423	-31.607	10.355	-0.953	-0.004	-0.001	0.001	0.234	-0.069	846.381	1.274	0.622	1.418

301.995	-33.579	10.971	-1.012	0.162	-0.023	0.001	0.256	-0.058	929.504	1.354	0.666	1.509
331.131	-27.007	11.552	-1.059	-1.818	-0.062	15.731	0.26	-0.089	1020.833	1.446	0.662	1.59
363.078	-41.656	13.691	-1.266	0.604	-0.08	0.001	0.306	-0.036	1120.681	1.55	0.752	1.723
398.107	-44.176	14.472	-1.341	0.817	-0.108	0.001	0.335	-0.019	1230.206	1.664	0.813	1.852

Table 3 Coefficients involved in equation (9).

f(hz)	c_0	c_1	c_2	c_3	c_4	c_5	c_6	c_7	c_8	c_9	φ	τ	σ
0.01	-19.748	3.009	-0.056	-0.021	-2.069	0.261	3.294	0	-0.709	0	0.784	0.388	0.875
0.011	-20.407	3.371	-0.085	-0.02	-1.991	0.248	3.325	0	-0.704	0	0.761	0.381	0.851
0.012	-20.712	3.52	-0.092	-0.016	-1.846	0.224	3.283	0	-0.732	0	0.78	0.399	0.876
0.013	-20.808	3.519	-0.093	-0.011	-1.824	0.224	3.065	0	-0.703	0	0.778	0.41	0.88
0.014	-19.938	3.334	-0.08	-0.013	-1.867	0.231	3.278	0	-0.706	0	0.789	0.423	0.895
0.016	-20.268	3.575	-0.1	-0.008	-1.834	0.223	3.111	0	-0.724	0	0.778	0.406	0.877
0.017	-19.871	3.492	-0.092	-0.014	-1.815	0.222	3.054	0	-0.732	0	0.781	0.412	0.883
0.019	-20.701	3.739	-0.109	0.003	-1.653	0.192	3.591	0	-0.706	0	0.771	0.428	0.882
0.021	-20.036	3.455	-0.076	-0.009	-1.446	0.16	3.555	0	-0.691	0	0.773	0.439	0.889
0.023	-20.137	3.601	-0.091	-0.005	-1.517	0.168	3.693	0	-0.681	0	0.765	0.438	0.881
0.025	-19.899	3.788	-0.115	-0.017	-1.648	0.186	3.743	0	-0.709	0	0.745	0.452	0.871
0.028	-21.328	4.241	-0.153	-0.007	-1.634	0.18	4.888	0	-0.651	0	0.724	0.433	0.843
0.03	-22.595	4.53	-0.161	-0.002	-1.325	0.123	4.913	0	-0.636	0	0.718	0.481	0.864
0.033	-22.71	4.529	-0.162	0.003	-1.344	0.128	4.528	0	-0.596	0	0.725	0.494	0.877
0.036	-22.312	4.527	-0.165	0.014	-1.469	0.142	5.844	0	-0.586	0	0.697	0.506	0.861
0.04	-22.823	4.836	-0.192	0.006	-1.509	0.143	6.215	0	-0.588	0	0.691	0.493	0.848
0.044	-23.981	5.306	-0.234	0.014	-1.548	0.147	6.442	0	-0.574	0	0.702	0.504	0.865
0.048	-24.315	5.405	-0.242	0.022	-1.489	0.135	6.314	0	-0.552	0	0.705	0.485	0.856
0.052	-24.759	5.582	-0.257	0.022	-1.443	0.129	6.138	0	-0.543	0	0.709	0.501	0.868
0.058	-24.297	5.571	-0.262	0.018	-1.565	0.145	7.33	0	-0.522	0	0.682	0.524	0.86
0.063	-24.448	5.829	-0.293	0.015	-1.695	0.163	7.201	0	-0.526	0	0.689	0.506	0.855
0.069	-25.088	6.046	-0.317	0.023	-1.717	0.168	7.433	0	-0.478	0	0.692	0.491	0.849
0.076	-25.508	6.215	-0.328	0.029	-1.609	0.15	7.425	0	-0.488	0	0.694	0.544	0.882
0.083	-25.486	6.37	-0.351	0.033	-1.733	0.171	7.574	0	-0.494	0	0.693	0.544	0.882
0.091	-23.585	5.959	-0.323	0.022	-1.828	0.184	8.325	0	-0.518	0	0.691	0.546	0.881
0.1	-23.162	5.95	-0.329	0.031	-1.904	0.198	7.939	0	-0.531	0	0.689	0.553	0.883
0.11	-22.737	5.914	-0.329	0.035	-1.881	0.197	6.912	0	-0.551	0	0.692	0.555	0.887
0.12	-21.288	5.586	-0.31	0.031	-1.987	0.217	6.7	0	-0.571	0	0.691	0.58	0.902
0.132	-22.022	5.9	-0.337	0.029	-1.904	0.204	7.179	0	-0.571	0	0.684	0.579	0.896
0.145	-20.656	5.61	-0.324	0.034	-2.027	0.227	6.373	0	-0.582	0	0.688	0.568	0.892
0.158	-21.491	5.913	-0.348	0.043	-1.927	0.211	6.31	0	-0.587	0	0.689	0.565	0.891
0.174	-21.748	6.043	-0.358	0.047	-1.786	0.191	5.662	0	-0.604	0	0.693	0.592	0.912
0.191	-22.301	6.278	-0.378	0.058	-1.649	0.17	5.139	0	-0.625	0	0.693	0.607	0.921

f(hz)	c_0	c_1	c_2	c_3	c_4	c_5	c_6	c_7	c_8	c_9	φ	τ	σ
0.209	-21.85	6.17	-0.37	0.061	-1.56	0.157	4.451	0	-0.63	0	0.702	0.604	0.926
0.229	-21.687	6.273	-0.384	0.066	-1.542	0.156	4.424	0	-0.669	0	0.717	0.613	0.944
0.251	-21.027	6.141	-0.376	0.073	-1.496	0.152	3.776	0	-0.7	0	0.733	0.625	0.963
0.275	-19.899	5.854	-0.356	0.086	-1.51	0.157	3.141	0	-0.724	0	0.76	0.628	0.986
0.302	-19.382	5.758	-0.351	0.1	-1.463	0.153	2.915	0	-0.752	0	0.779	0.638	1.007
0.331	-18.741	5.684	-0.352	0.095	-1.508	0.16	2.943	0	-0.762	0	0.79	0.616	1.002
0.363	-18.707	5.711	-0.358	0.108	-1.485	0.155	3.157	0	-0.749	0	0.793	0.578	0.981
0.398	-18.872	5.874	-0.374	0.122	-1.44	0.142	3.692	0	-0.768	0	0.785	0.541	0.953
0.437	-18.431	5.86	-0.374	0.127	-1.398	0.132	3.446	0	-0.807	0	0.784	0.507	0.933
0.479	-18.189	5.779	-0.367	0.144	-1.318	0.117	3.545	0	-0.805	0	0.795	0.481	0.93
0.525	-16.311	5.199	-0.323	0.155	-1.351	0.124	3.339	0	-0.811	0	0.787	0.459	0.911
0.575	-16.063	5.189	-0.327	0.16	-1.338	0.123	3.286	0	-0.817	0	0.769	0.445	0.888
0.631	-15.596	5.058	-0.312	0.167	-1.216	0.102	2.986	0	-0.849	0	0.766	0.423	0.875
0.692	-14.583	4.832	-0.291	0.178	-1.121	0.085	3.069	0	-0.917	0	0.768	0.409	0.87
0.759	-13.97	4.74	-0.284	0.177	-1.105	0.077	3.199	0	-0.938	0.084	0.748	0.403	0.849
0.832	-13.756	4.621	-0.277	0.191	-1.138	0.077	3.95	0	-0.883	0	0.733	0.389	0.829
0.912	-13.342	4.508	-0.268	0.197	-1.096	0.067	3.446	0	-0.877	0.497	0.718	0.381	0.813
1	-12.532	4.292	-0.257	0.218	-1.183	0.083	3.86	0	-0.876	1.178	0.7	0.384	0.798
1.096	-12.906	4.505	-0.278	0.225	-1.164	0.075	4.629	0	-0.886	1.339	0.701	0.369	0.792
1.202	-12.643	4.344	-0.259	0.243	-1.033	0.047	4.743	0	-0.866	2.429	0.682	0.386	0.784
1.318	-12.157	4.146	-0.248	0.264	-1.099	0.061	4.276	0	-0.838	2.781	0.682	0.38	0.781
1.445	-11.11	3.753	-0.216	0.272	-1.152	0.064	5.274	0	-0.801	2.047	0.674	0.372	0.77
1.585	-12.977	4.096	-0.24	0.3	-0.996	0.034	5.552	0	-0.687	3.382	0.666	0.37	0.762
1.738	-13.097	4.058	-0.232	0.317	-0.977	0.021	6.099	0	-0.639	4.242	0.67	0.362	0.762
1.905	-13.129	3.989	-0.229	0.342	-0.977	0.021	5.941	0	-0.597	5.248	0.638	0.378	0.741
2.089	-11.909	3.664	-0.215	0.35	-1.142	0.049	6.856	0	-0.568	5.673	0.628	0.337	0.713
2.291	-11.848	3.42	-0.189	0.373	-1.102	0.032	7.694	0	-0.467	5.721	0.605	0.322	0.685
2.512	-13.106	3.644	-0.213	0.412	-1.04	0.031	6.55	0	-0.404	7.794	0.609	0.315	0.685
2.754	-11.932	3.032	-0.157	0.43	-0.999	0.016	7.229	0	-0.316	8.544	0.571	0.295	0.643
3.02	-10.581	2.718	-0.139	0.46	-1.191	0.046	7.283	0	-0.345	9.691	0.556	0.294	0.629
3.311	-10.01	2.466	-0.123	0.45	-1.241	0.061	7.701	0.002	-0.286	10.089	0.534	0.284	0.604
3.631	-9.548	2.183	-0.104	0.487	-1.271	0.067	8.216	0.002	-0.229	11.99	0.533	0.283	0.604
3.981	-10.123	2.358	-0.109	0.526	-1.12	0.025	10.778	0.002	-0.238	14.209	0.546	0.226	0.591
4.365	-8.593	1.961	-0.092	0.532	-1.413	0.066	11.695	0.001	-0.184	15.103	0.514	0.227	0.562
4.786	-9.72	2.3	-0.124	0.532	-1.356	0.067	11.289	0.004	-0.166	15.941	0.469	0.213	0.516
5.248	-10.135	2.34	-0.13	0.548	-1.288	0.067	11.559	0.005	-0.14	18.291	0.485	0.194	0.523
5.754	-9.894	2.349	-0.134	0.563	-1.513	0.075	14.732	0.004	-0.075	19.793	0.488	0.188	0.523
6.31	-10.342	2.367	-0.146	0.598	-1.496	0.094	14.361	0.006	-0.042	22.505	0.481	0.161	0.507
6.918	-10.436	2.454	-0.151	0.585	-1.606	0.084	15.344	0.004	0.004	23.147	0.493	0.187	0.528
7.586	-10.471	2.103	-0.123	0.6	-1.55	0.089	14.276	0.005	0.113	24.129	0.478	0.203	0.519
8.318	-11.363	2.165	-0.126	0.627	-1.328	0.064	12.888	0.007	0.144	27.088	0.483	0.161	0.509

f(hz)	c_0	c_1	c_2	c_3	c_4	c_5	c_6	c_7	c_8	c_9	φ	τ	σ
9.12	-10.303	1.807	-0.108	0.622	-1.428	0.096	11.952	0.008	0.159	29.267	0.465	0.208	0.509
10	-11.069	1.982	-0.13	0.646	-1.591	0.124	12.448	0.008	0.219	31.166	0.434	0.221	0.487
10.965	-11.005	2.023	-0.14	0.658	-1.63	0.134	12.63	0.008	0.185	33.581	0.45	0.16	0.478
12.023	-10.398	1.995	-0.128	0.65	-1.633	0.102	14.427	0.007	0.154	36.176	0.481	0.102	0.492
13.183	-10.189	1.853	-0.123	0.639	-1.523	0.115	12.485	0.009	0.117	40.392	0.468	0.149	0.492
14.454	-9.645	1.687	-0.109	0.651	-1.553	0.115	12.253	0.009	0.111	44.085	0.462	0.129	0.48
15.849	-10.11	1.889	-0.123	0.68	-1.438	0.104	11.443	0.01	0.027	49.573	0.477	0.109	0.489
17.378	-11.459	2.125	-0.146	0.67	-1.344	0.109	9.346	0.012	0.078	53.57	0.46	0.133	0.479
19.055	-11.603	2.049	-0.133	0.659	-1.094	0.087	8.604	0.015	0.053	58.054	0.462	0.111	0.475
20.893	-12.723	2.284	-0.152	0.654	-1.036	0.083	7.878	0.017	0.105	62.817	0.471	0.121	0.486
22.909	-11.547	2.04	-0.133	0.656	-1.072	0.092	7.392	0.019	0.031	69.18	0.467	0.147	0.489
25.119	-11.83	2.094	-0.136	0.672	-1.084	0.086	7.24	0.02	0.058	77.615	0.504	0.138	0.522
27.542	-11.359	2.217	-0.151	0.678	-1.232	0.091	10.29	0.021	0.025	86.343	0.484	0.133	0.501
30.2	-12.36	2.505	-0.167	0.666	-1.101	0.069	10.177	0.024	0.017	94.592	0.468	0.138	0.488
33.113	-11.845	2.518	-0.171	0.657	-1.198	0.074	10.221	0.026	-0.002	103.996	0.461	0.158	0.487
36.308	-11.046	2.335	-0.158	0.639	-1.225	0.08	9.433	0.028	-0.018	114.064	0.477	0.133	0.495
39.811	-10.64	2.519	-0.173	0.628	-1.399	0.08	11.468	0.03	-0.044	125.569	0.471	0.149	0.494
43.652	-10.474	2.643	-0.181	0.611	-1.451	0.074	11.585	0.032	-0.076	138.293	0.491	0.169	0.519
47.863	-7.157	1.97	-0.151	0.543	-1.958	0.159	12.113	0.035	-0.11	150.121	0.578	0.236	0.624
52.481	-11.251	2.539	-0.172	0.614	-1.26	0.068	11.503	0.04	-0.015	164.497	0.518	0.176	0.547
57.544	-11.62	2.7	-0.188	0.611	-1.258	0.066	11.627	0.044	-0.013	180.279	0.528	0.182	0.558
63.096	-12.024	2.875	-0.206	0.609	-1.255	0.064	11.747	0.049	-0.012	197.575	0.539	0.189	0.571
69.183	-12.453	3.063	-0.225	0.606	-1.257	0.062	11.888	0.054	-0.011	216.554	0.553	0.197	0.587
75.858	-12.971	3.279	-0.246	0.602	-1.252	0.059	12.026	0.059	-0.009	237.367	0.568	0.206	0.604
83.176	-13.523	3.513	-0.269	0.599	-1.249	0.056	12.169	0.065	-0.008	260.172	0.585	0.216	0.624
91.201	-14.123	3.771	-0.294	0.595	-1.248	0.053	12.317	0.071	-0.006	285.189	0.605	0.228	0.647
100	-14.77	4.048	-0.322	0.591	-1.246	0.049	12.47	0.078	-0.004	312.615	0.628	0.241	0.672
109.648	-15.474	4.353	-0.352	0.586	-1.246	0.045	12.626	0.086	-0.002	342.686	0.654	0.255	0.702
120.226	-16.255	4.69	-0.385	0.581	-1.245	0.041	12.782	0.094	0	375.665	0.683	0.271	0.735
131.826	-17.085	5.054	-0.421	0.575	-1.247	0.036	12.951	0.104	0.003	411.816	0.716	0.289	0.773
144.544	-18.018	5.46	-0.462	0.569	-1.247	0.031	13.119	0.114	0.005	451.468	0.754	0.309	0.815
158.489	-22.999	6.054	-0.527	0.568	-0.357	0.043	0.012	0.135	0.035	495.105	0.796	0.36	0.874
173.78	-24.959	6.73	-0.591	0.561	-0.25	0.03	0.002	0.147	0.04	542.763	0.843	0.385	0.927
190.546	-27.569	7.618	-0.672	0.554	-0.09	0.01	0.001	0.162	0.042	595.128	0.898	0.409	0.987
208.93	-22.651	7.507	-0.664	0.537	-1.262	0.003	13.835	0.165	0.018	652.186	0.957	0.413	1.042
229.087	-24.105	8.149	-0.727	0.526	-1.267	-0.005	13.993	0.181	0.022	715.021	1.024	0.446	1.117
251.189	-33.289	9.583	-0.86	0.523	0.248	-0.035	0.001	0.211	0.061	783.996	1.096	0.519	1.213
275.423	-35.84	10.458	-0.943	0.51	0.398	-0.054	0.001	0.232	0.068	859.386	1.178	0.562	1.305
301.995	-29.241	10.475	-0.956	0.49	-1.312	-0.038	14.575	0.239	0.037	942.32	1.273	0.566	1.393
331.131	-40.405	11.989	-1.09	0.483	0.732	-0.098	0.001	0.277	0.083	1033.049	1.37	0.665	1.523
363.078	-33.557	12.437	-1.149	0.46	-1.353	-0.065	14.934	0.287	0.049	1132.783	1.487	0.666	1.629

f(hz)	c_0	c_1	c_2	c_3	c_4	c_5	c_6	c_7	c_8	c_9	φ	τ	σ
398.107	-47.653	14.461	-1.323	0.451	1.171	-0.155	0.001	0.333	0.103	1241.767	1.607	0.781	1.787

Table 4 Coefficients involved in equation (15).

f_{osc}(hz)	d_0	d_1	d_2	d_3	d_4	φ	τ	σ
0.2	-49.556	11.539	0.236	0.508	0	0.793	0.45	0.912
0.219	-46.82	10.891	0.246	0.245	0	0.788	0.439	0.902
0.24	-47.284	11.005	0.254	0.701	0	0.762	0.427	0.874
0.264	-49.302	11.493	0.309	0.679	-0.001	0.771	0.426	0.881
0.289	-48.161	11.392	0.308	0.443	-0.002	0.739	0.446	0.863
0.317	-36.577	9.835	0.281	0.503	-0.007	0.721	0.471	0.862
0.348	-32.972	9.164	0.27	0.45	-0.006	0.692	0.47	0.837
0.381	-29.813	8.441	0.261	0.497	-0.006	0.679	0.468	0.825
0.418	-23.998	7.326	0.242	0.494	-0.006	0.664	0.444	0.799
0.458	-17.785	6.092	0.224	0.518	-0.006	0.647	0.408	0.765
0.502	-14.46	5.366	0.209	0.549	-0.006	0.634	0.385	0.742
0.551	-9.849	4.431	0.193	0.541	-0.006	0.621	0.359	0.718
0.604	-6.446	3.723	0.174	0.539	-0.006	0.601	0.346	0.693
0.662	-4.964	3.35	0.158	0.743	-0.005	0.585	0.341	0.677
0.726	-2.114	2.772	0.141	0.787	-0.005	0.578	0.322	0.662
0.796	-0.627	2.428	0.124	0.878	-0.005	0.568	0.314	0.649
0.873	0.769	2.088	0.11	0.902	-0.005	0.552	0.3	0.628
0.957	2.08	1.726	0.101	1.002	-0.005	0.543	0.285	0.613
1.05	2.267	1.572	0.094	0.933	-0.004	0.528	0.275	0.595
1.151	2.065	1.484	0.089	0.856	-0.004	0.507	0.271	0.575
1.262	1.05	1.56	0.082	0.761	-0.003	0.491	0.271	0.561
1.384	0.343	1.597	0.077	0.688	-0.003	0.479	0.271	0.55
1.517	-0.182	1.596	0.074	0.557	-0.003	0.47	0.266	0.54
1.664	-0.45	1.558	0.072	0.45	-0.003	0.467	0.262	0.536
1.824	-0.754	1.545	0.071	0.269	-0.002	0.465	0.262	0.534
2	-0.624	1.451	0.071	0.083	-0.002	0.461	0.26	0.529
2.193	-0.082	1.301	0.069	0.129	-0.002	0.456	0.263	0.526
2.405	0.078	1.239	0.066	0.264	-0.002	0.457	0.261	0.526
2.637	0.108	1.189	0.065	0.405	-0.002	0.457	0.265	0.528
2.891	0.308	1.086	0.066	0.515	-0.002	0.459	0.273	0.534
3.17	0.452	1.005	0.068	0.683	-0.002	0.457	0.284	0.538
3.476	0.21	0.999	0.071	0.695	-0.002	0.451	0.292	0.537
3.811	-0.175	1.022	0.073	0.53	-0.002	0.455	0.299	0.544
4.179	-0.483	1.037	0.076	0.258	-0.002	0.457	0.304	0.549
4.582	-0.851	1.069	0.078	0.216	-0.002	0.461	0.301	0.55

f_{osc}(hz)	d_0	d_1	d_2	d_3	d_4	φ	τ	σ
5.024	-1.319	1.121	0.08	0.163	-0.002	0.467	0.298	0.554
5.508	-1.638	1.138	0.084	0.129	-0.002	0.468	0.308	0.561
6.04	-1.738	1.115	0.088	0.008	-0.002	0.463	0.323	0.565
6.623	-2.136	1.154	0.092	0.318	-0.001	0.46	0.33	0.566
7.262	-2.558	1.203	0.096	0.554	-0.001	0.454	0.329	0.561
7.962	-2.97	1.261	0.1	1.022	-0.001	0.452	0.326	0.557
8.73	-3.354	1.314	0.103	1.24	-0.001	0.446	0.329	0.554
9.573	-3.957	1.433	0.106	1.058	-0.002	0.448	0.329	0.556
10.496	-4.225	1.468	0.108	1.304	-0.002	0.452	0.316	0.551
11.509	-4.386	1.489	0.109	1.404	-0.002	0.461	0.317	0.56
12.619	-4.377	1.456	0.11	2.183	-0.002	0.463	0.328	0.567
13.837	-4.469	1.461	0.111	2.452	-0.002	0.47	0.333	0.576
15.172	-4.492	1.448	0.114	3.023	-0.001	0.475	0.337	0.583
16.635	-4.268	1.419	0.11	3.912	-0.002	0.489	0.34	0.596
18.24	-4.182	1.403	0.109	3.763	-0.001	0.489	0.349	0.601
20	-3.873	1.361	0.107	3.572	-0.002	0.491	0.344	0.6
21.93	-4.211	1.369	0.104	2.656	-0.001	0.459	0.397	0.607

Table 5 Coefficients involved in equation (16).

f_{osc} (hz)	d_0	d_1	d_2	d_3	d_4	d_5	φ	τ	σ
0.2	-48.914	11.406	0.231	0	0	8.824	0.793	0.449	0.911
0.219	-46.791	10.822	0.238	1.034	0	14.885	0.788	0.439	0.902
0.24	-46.7	10.854	0.248	0.274	-0.001	13.885	0.762	0.428	0.873
0.264	-48.91	11.397	0.304	0.144	-0.002	6.687	0.771	0.424	0.88
0.289	-48.703	11.367	0.307	0.747	-0.002	12.368	0.74	0.443	0.862
0.317	-37.393	9.882	0.281	0.511	-0.006	10.823	0.722	0.469	0.861
0.348	-33.352	9.19	0.27	0.454	-0.006	4.59	0.693	0.469	0.837
0.381	-30.05	8.449	0.261	0.485	-0.006	3.558	0.679	0.467	0.825
0.418	-24.782	7.384	0.242	0.5	-0.006	9.064	0.665	0.442	0.798
0.458	-19.345	6.204	0.224	0.527	-0.005	18.292	0.648	0.405	0.764
0.502	-16.98	5.517	0.209	0.581	-0.005	33.84	0.635	0.379	0.74
0.551	-12.741	4.592	0.193	0.58	-0.005	40.855	0.622	0.352	0.714
0.604	-9.759	3.888	0.175	0.614	-0.005	49.204	0.601	0.336	0.689
0.662	-8.759	3.519	0.159	0.766	-0.004	58.012	0.585	0.326	0.67
0.726	-5.689	2.924	0.142	0.873	-0.005	56.074	0.578	0.308	0.655
0.796	-3.793	2.537	0.125	0.977	-0.005	53.275	0.568	0.3	0.642
0.873	-2.139	2.191	0.111	0.98	-0.004	48.353	0.552	0.287	0.622
0.957	-0.749	1.839	0.102	1.154	-0.004	46.129	0.542	0.272	0.607
1.05	-0.473	1.668	0.096	1.101	-0.004	45.958	0.527	0.261	0.588

1.151	-0.832	1.584	0.09	1.035	-0.003	50.579	0.505	0.254	0.565
1.262	-1.987	1.666	0.083	0.904	-0.003	53.105	0.488	0.252	0.549
1.384	-2.705	1.699	0.077	0.848	-0.002	53.733	0.475	0.25	0.537
1.517	-3.222	1.7	0.074	0.706	-0.002	53.655	0.465	0.245	0.525
1.664	-3.412	1.654	0.072	0.518	-0.002	53.144	0.461	0.242	0.521
1.824	-3.659	1.634	0.07	0.347	-0.002	53.016	0.458	0.241	0.518
2	-3.359	1.522	0.07	0.236	-0.002	52.071	0.454	0.239	0.513
2.193	-2.807	1.381	0.068	0.259	-0.002	50.955	0.449	0.241	0.509
2.405	-2.619	1.32	0.065	0.379	-0.002	50.447	0.449	0.238	0.509
2.637	-2.612	1.276	0.064	0.562	-0.002	50.261	0.449	0.242	0.51
2.891	-2.343	1.172	0.065	0.586	-0.002	48.787	0.451	0.251	0.516
3.17	-2.197	1.099	0.067	0.865	-0.001	47.715	0.448	0.263	0.519
3.476	-2.409	1.086	0.07	0.96	-0.001	47.791	0.441	0.271	0.518
3.811	-2.708	1.098	0.072	0.716	-0.001	47.428	0.445	0.279	0.525
4.179	-2.896	1.102	0.075	0.528	-0.001	46.441	0.447	0.285	0.53
4.582	-3.174	1.127	0.077	0.337	-0.001	46.044	0.451	0.281	0.531
5.024	-3.641	1.177	0.078	0.374	-0.001	46.838	0.458	0.275	0.534
5.508	-3.961	1.198	0.082	0.326	-0.001	46.801	0.46	0.281	0.539
6.04	-3.954	1.168	0.086	0.377	-0.001	45.435	0.456	0.294	0.542
6.623	-4.224	1.198	0.091	0.596	-0.001	42.911	0.454	0.299	0.544
7.262	-4.481	1.227	0.095	1.192	-0.001	41.508	0.45	0.298	0.54
7.962	-4.706	1.266	0.099	1.605	-0.001	39.302	0.448	0.298	0.538
8.73	-4.885	1.306	0.102	1.591	-0.001	36.787	0.444	0.302	0.537
9.573	-5.01	1.33	0.105	2.009	-0.001	34.282	0.447	0.302	0.54
10.496	-5.177	1.423	0.108	1.756	-0.001	27.511	0.452	0.296	0.54
11.509	-5.273	1.438	0.109	1.882	-0.001	26.68	0.463	0.296	0.549
12.619	-5.289	1.412	0.111	2.772	-0.001	26.531	0.465	0.308	0.558
13.837	-5.39	1.412	0.113	3.212	-0.001	27.014	0.472	0.312	0.566
15.172	-5.445	1.413	0.115	2.624	-0.001	27.233	0.477	0.316	0.573
16.635	-5.86	1.384	0.113	5.156	-0.001	42.718	0.492	0.303	0.578
18.24	-5.806	1.384	0.113	4.858	-0.001	41.486	0.493	0.311	0.583
20	-5.47	1.37	0.111	4.374	-0.001	36.57	0.495	0.312	0.585
21.93	-5.182	1.353	0.107	3.075	-0.001	27.869	0.462	0.379	0.597

Table 6 Coefficients involved in equation (17).

fosc(hz)	d_0	d_1	d_2	d_3	d_4	d_5	d_6	φ	τ	σ
0.2	-48.453	11.522	-0.002	0.201	5.135	-0.002	37.537	0.78	0.429	0.89
0.219	-40.021	9.868	-0.002	0.216	0.775	-0.004	42.153	0.776	0.407	0.876
0.24	-40.668	9.948	-0.002	0.228	4.467	-0.004	45.647	0.75	0.398	0.849
0.264	-42.6	10.616	-0.002	0.286	0.914	-0.005	20.19	0.755	0.42	0.864

0.289	-42.394	10.589	-0.002	0.282	0	-0.006	36.57	0.723	0.435	0.843
0.317	-40.594	10.335	-0.002	0.258	0.381	-0.007	60.921	0.707	0.458	0.843
0.348	-34.297	9.454	-0.002	0.248	3.297	-0.007	34.26	0.677	0.469	0.824
0.381	-28.936	8.493	-0.002	0.236	0.277	-0.008	25.636	0.667	0.468	0.815
0.418	-29.563	8.614	-0.002	0.23	0.248	-0.007	15.843	0.651	0.452	0.792
0.458	-19.347	6.226	-0.002	0.21	0.666	-0.006	47.683	0.637	0.404	0.755
0.502	-19.481	5.857	-0.002	0.198	0.57	-0.005	80.695	0.623	0.379	0.73
0.551	-14.78	4.856	-0.002	0.183	0.541	-0.005	85.837	0.609	0.353	0.704
0.604	-9.424	3.795	-0.002	0.163	0.467	-0.005	78.717	0.589	0.338	0.679
0.662	-10.07	3.642	-0.002	0.149	1.25	-0.004	103.348	0.573	0.328	0.66
0.726	-6.758	2.95	-0.002	0.132	0.974	-0.005	104.787	0.567	0.307	0.645
0.796	-4.683	2.604	-0.001	0.118	1.317	-0.005	88.204	0.558	0.299	0.633
0.873	-2.871	2.221	-0.001	0.106	1.501	-0.004	81.521	0.543	0.285	0.613
0.957	-1.452	1.876	-0.001	0.097	1.025	-0.004	76.819	0.535	0.268	0.598
1.05	-1.312	1.725	-0.001	0.091	1.706	-0.004	76.29	0.519	0.256	0.578
1.151	-1.428	1.618	-0.001	0.085	1.118	-0.003	78.392	0.496	0.247	0.554
1.262	-2.775	1.737	-0.001	0.079	1.233	-0.003	80.619	0.478	0.242	0.536
1.384	-3.694	1.799	-0.001	0.073	0	-0.002	81.846	0.464	0.239	0.522
1.517	-4.002	1.775	-0.001	0.07	1.003	-0.002	80.064	0.453	0.234	0.51
1.664	-4.006	1.704	-0.001	0.068	0.831	-0.002	77.29	0.45	0.23	0.506
1.824	-4.333	1.703	-0.001	0.067	0.82	-0.002	75.298	0.449	0.23	0.504
2	-3.904	1.567	-0.001	0.066	0.015	-0.002	73.619	0.445	0.228	0.5
2.193	-3.282	1.421	-0.001	0.065	0.516	-0.002	70.455	0.441	0.232	0.498
2.405	-3.243	1.405	-0.001	0.061	0.198	-0.002	68.399	0.444	0.227	0.498
2.637	-3.119	1.324	0	0.061	0.341	-0.002	62.989	0.446	0.234	0.504
2.891	-3.765	1.412	0	0.06	0	-0.001	61.531	0.45	0.239	0.509
3.17	-2.754	1.194	-0.001	0.063	1.834	-0.001	60.138	0.445	0.251	0.511
3.476	-2.254	1.159	-0.001	0.067	0.042	-0.002	44.964	0.438	0.263	0.511
3.811	-3.6	1.248	0	0.069	0.705	-0.001	57.705	0.443	0.267	0.518
4.179	-3.525	1.205	0	0.07	0	-0.001	56.034	0.445	0.274	0.522
4.582	-3.656	1.284	-0.001	0.072	0.705	-0.001	48.783	0.447	0.267	0.52
5.024	-4.251	1.237	-0.001	0.074	0	-0.001	66.007	0.452	0.258	0.521
5.508	-4.152	1.192	-0.001	0.077	0	-0.001	65.172	0.453	0.265	0.525
6.04	-4.062	1.156	-0.001	0.082	1.537	-0.001	61.947	0.449	0.276	0.526
6.623	-4.324	1.178	-0.001	0.086	0.61	-0.001	60.781	0.448	0.279	0.528
7.262	-4.738	1.227	-0.001	0.09	2.029	-0.001	59.875	0.446	0.275	0.524
7.962	-4.826	1.239	-0.001	0.093	0.203	-0.001	59.755	0.446	0.268	0.52
8.73	-5.021	1.267	-0.001	0.097	2.215	-0.001	58.881	0.442	0.272	0.518
9.573	-5.213	1.289	-0.001	0.1	2.009	-0.001	59.054	0.445	0.271	0.521
10.496	-4.963	1.342	-0.001	0.102	0	-0.001	44.739	0.45	0.268	0.524
11.509	-5.552	1.409	-0.001	0.105	2.678	-0.001	47.798	0.46	0.266	0.532
12.619	-6.472	1.496	-0.001	0.109	4.137	-0.001	56.259	0.465	0.277	0.541

13.837	-6.516	1.508	-0.001	0.11	2.61	-0.001	56.102	0.472	0.283	0.55
15.172	-6.484	1.495	-0.001	0.114	4.274	-0.001	51.836	0.476	0.29	0.558
16.635	-6.776	1.468	-0.001	0.113	6.029	-0.001	62.664	0.49	0.29	0.569
18.24	-6.225	1.454	-0.001	0.11	3.56	-0.001	54.951	0.489	0.303	0.576
20	-6.054	1.444	-0.001	0.109	4.195	-0.001	53.1	0.492	0.302	0.577
21.93	-6.362	1.514	-0.001	0.106	1.632	-0.001	46.148	0.462	0.367	0.59